Downloaded from rsta.royalsocietypublishing.org

PHILOSOPHICAL TRANSACTIONS OF THE ROYAL SOCIETY A MATHEMATICAL, PHYSICAL & ENGINEERING SCIENCES

Attractive Dislocation Intersections and Work Hardening in Metals

J. D. Baird and B. Gale

Phil. Trans. R. Soc. Lond. A 1965 **257**, 553-590
doi: 10.1098/rsta.1965.0015

Email alerting service

Receive free email alerts when new articles cite this article - sign up in the box at the top right-hand corner of the article or click **here**

To subscribe to *Phil. Trans. R. Soc. Lond. A* go to: **http://rsta.royalsocietypublishing.org/subscriptions**

This journal is © 1965 The Royal Society

Downloaded from rsta.royalsocietypublishing.org

ATTRACTIVE DISLOCATION INTERSECTIONS AND WORK HARDENING IN METALS

By J. D. BAIRD† and B. GALE

National Physical Laboratory, Teddington, Middlesex

(*Communicated by N. P. Allen, F.R.S.—Received* 10 *February* 1964—
Revised 22 *September* 1964)

CONTENTS

The behaviour of two intersecting dislocations in a stressed crystal is discussed in relation to the problem of work hardening. It is assumed that the crystal is elastically isotropic and the effects of changing the applied stress and the Burgers vectors of the dislocations are examined in detail. Quantitative estimates of the yield stress as a function of the dislocation distribution are made and compared with experimental results. It is deduced, qualitatively, that the mechanism is probably an important factor in describing the temperature dependance of the flow stress, the orientation dependence of work hardening, the Bauschinger effect and the formation of cell walls.

Introduction

Many mechanisms have been suggested which could contribute to work hardening in metals; for example, elastic interaction of dislocations on parallel glide planes, the formation of sessile dislocations and the formation of jogs by intersections or cross-slip. To determine

† Now at Central Research Department, Colvilles Ltd.

Vol. 257. A. 1087. (Price 15*s*.; U.S. $2.25) 68 [Published 17 June 1965

The Royal Society is collaborating with JSTOR to digitize, preserve, and extend access to
Philosophical Transactions of the Royal Society of London. Series A, Mathematical and Physical Sciences.
www.jstor.org

Downloaded from rsta.royalsocietypublishing.org

the relative importance of each mechanism it is necessary to calculate the magnitude and characteristics of the contribution which each is expected to make to the flow stress of a work-hardened metal and then to compare the result with experimental observations.

One mechanism of hardening which must exist in metals where numerous slip systems are operative is the elastic or long-range interaction between dislocations moving on different glide planes at or near the points where they intersect. Depending upon the respective Burgers vectors of these intersecting dislocations such intersections may be repulsive or attractive. From a simple physical argument (Carrington, Hale & McLean 1960) it can be deduced that the attractive intersections must be stronger. The energy of the dislocation system is lowered when two dislocations which attract each other approach, whereas it is increased by the approach of two dislocations which repel each other. In the attractive case the dislocations will bend in order to lie more nearly parallel and so decrease the total energy, but in the repulsive case they will bend so as to cross orthogonally in order to minimize the increase in energy. This simple conclusion has been substantiated by a calculation by Saada (1960*b*) and it is therefore considered that the main contribution to the flow stresses from an intersection mechanism should come from attractive junctions.

Approximate analyses of attractive intersections have been made by Friedel (1959), Thornton (1959) and Carrington *et al.* (1960). These authors only made simple calculations of the release of energy when an attractive reaction occurs and they did not consider the subsequent behaviour when stress is applied to the crystal containing it. This is an important omission, for the dislocation intersection cannot be broken without stress and, in most cases, considerably more work must be done by the stress to break it than was released in forming it. The simple calculation thus tends to underestimate the average strength of these configurations by a factor of 2 or 3. Saada (1960*a*) and Baird & Gale (1960) have given analyses of some sessile intersections in face-centred cubic metals in which the behaviour under particular stress conditions was considered.

This paper describes the behaviour of both sessile and glissile junctions in face-centred cubic metals and the behaviour of sessile junctions in body-centred cubic crystals. Some of the results for the face-centred cubic case are also applicable to hexagonal close-packed metals. The first part describes the geometry and dynamics of the model and the results of the calculations; the second part discusses some ideas of the way in which this mechanism may influence work hardening. Details of mathematical procedures used in the calculations are given in appendices.

I. THE GEOMETRY AND DYNAMICS OF THE MECHANISM

1. Initial reaction

In figure 1 two straight dislocation line segments are shown bounded by pairs of pinning points A_1, A_1' and A_2, A_2'. The segment A_1A_1' has a Burgers vector $\mathbf{b}(1)$ and lies in a slip plane with normal $\mathbf{n}(1)$ and the segment A_2A_2' has a Burgers vector $\mathbf{b}(2)$ and lies in a slip plane with normal $\mathbf{n}(2)$. These pinning points may be inclusions or, more likely, the nodes of a dislocation 'forest' or network. Their exact nature is not discussed here and it is only assumed that they are rigid. The dislocations intersect at a point F, on the line of intersection $\mathbf{l}(12)$, of the two slip planes and they are inclined to this line at angles ϕ_1 and ϕ_2:

Downloaded from rsta.royalsocietypublishing.org

with $-\frac{1}{2}\pi \leqslant \phi_1, \phi_2 \leqslant +\frac{1}{2}\pi$. For certain pairs of Burgers vectors and certain ranges of ϕ_1, and ϕ_2 the total energy of this configuration will decrease if the configuration changes and becomes two pairs of straight segments; A_1P_0 and $A_1'Q_0$ having Burgers vector $\mathbf{b}(1)$, A_2P_0 and $A_2'Q_0$ having Burgers vector $\mathbf{b}(2)$; and the straight segment P_0Q_0 having a Burgers vector; $\mathbf{b}(12) = \mathbf{b}(1)+\mathbf{b}(2)$.

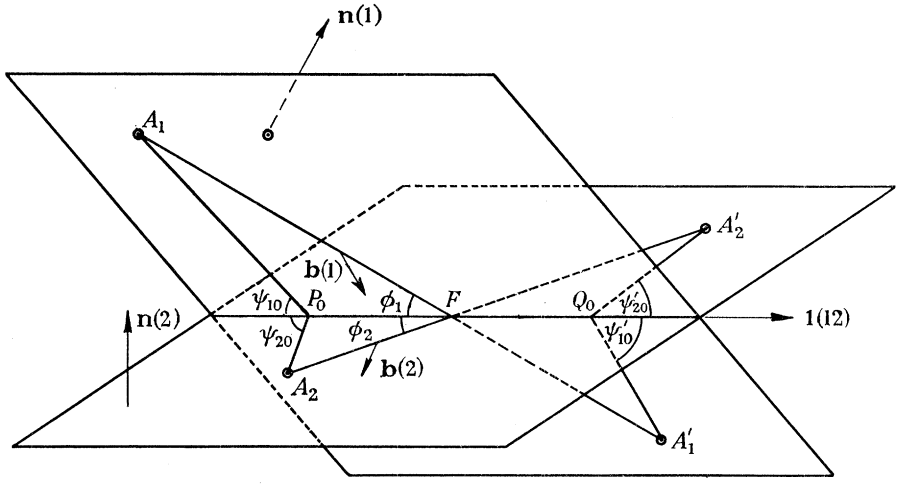

FIGURE 1. The dislocation and slip plane configuration when the applied stress is zero.

In an isotropic crystal the line energies per unit length are given by the relation

$$E = \frac{G|\mathbf{b}|^2}{4\pi(1-\nu)} \ln\left(\frac{r_1}{r_0}\right)(1-\nu\cos^2\alpha); \tag{1}$$

G is the shear modulus, ν is Poisson's ratio, r_1 and r_0 are integration limits and α is the angle between the Burgers vector and the tangent to the dislocation line. If E_1, E_2 and E_{12} are respectively the line energies of the dislocations A_1A_1', A_2A_2' and P_0Q_0 it is easily shown that the reaction will occur if

$$E_1\cos\phi_1 + E_2\cos\phi_2 > E_{12}, \tag{2}$$

and that the energy of the configuration is a minimum when the equation

$$E_1\cos\psi_{10} + E_2\cos\psi_{20} = E_{12} \tag{3}$$

is satisfied at P_0 and a similar equation is satisfied at Q_0.

The inequality (2) can be used to classify the possible reactions in face-centred cubic, body-centred cubic and hexagonal crystals, but it is simple only if the variation of E with α is ignored. This assumption is not unreasonable since the factor containing 'α' in equation (1) is slowly varying. This being so the classification can be briefly summarized as follows.

(*a*) *Face-centred cubic*

In these crystals the Burgers vectors and slip planes of the reacting dislocations A_1A_1' and A_2A_2' are of the form $\frac{1}{2}a\langle 01\bar{1}\rangle$ and $\{111\}$; here a is the size of the cubic cell. If the slip plane and slip direction of the dislocation A_1A_1' are chosen there are eighteen possible reactions between it and all other dislocations A_2A_2' on different slip planes. There are five distinct types of reaction. There are four cases where $\mathbf{b}(1)$ and $\mathbf{b}(2)$ are perpendicular and no reaction occurs, one case where $\mathbf{b}(1)$ and $\mathbf{b}(2)$ are antiparallel and annihilation

Downloaded from rsta.royalsocietypublishing.org

occurs and seven cases where the dislocations repel each other. In the remaining six cases the dislocations attract and the inequality (2) can be satisfied. For two of these attractive reactions the slip plane of P_0Q_0 is of the form {100}. This is not a common slip plane of the lattice and because of the stacking fault configuration adopted the dislocation should not move when a shear stress is applied. This configuration is called sessile. In the remaining four of the six attractive reactions the slip plane of P_0Q_0 is either coincident with $\mathbf{n}(1)$ or with $\mathbf{n}(2)$ and it may become curved under stress. This configuration is called glissile. If the slip plane and the slip direction of A_1A_1' can have all the 24 possible values there will be 216 possible reactions in a particular crystal of which 24 are sessile, 48 are glissile and 144 are not attractive.

(*b*) *Hexagonal close packed*

Slip dislocations in this system are thought to have Burgers vectors which are predominantly of the form $\frac{1}{3}a\langle 11\bar{2}0\rangle$. These will tend to move in the basal plane, where the energy is reduced by dissociation into half dislocations, as in the face-centred cubic lattice. However slip on the $\{10\bar{1}0\}$ prismatic planes and on the $\{10\bar{1}1\}$ pyramidal planes is also observed with the same slip vector; especially in titanium (Barrett 1953). If the Burgers vector of the dislocation A_1A_1' is chosen there will be six sets of reactions corresponding to the six different values of the Burgers vector of the dislocation A_2A_2'. In three cases there will be repulsion, in one case annihilation and in two cases an attractive reaction of the type considered in this paper will occur. The set of attractive reactions can itself be divided into five sets in all of which the resultant dislocation P_0Q_0 has a Burgers vector of the form $\frac{1}{3}a\langle 11\bar{2}0\rangle$: here a is the length of a side of the basal hexagon. These reactions are listed below: the slip plane of P_0Q_0 is parallel to the vector $\mathbf{b}(12)\wedge\mathbf{l}(12)$ and is denoted by $\mathbf{n}(12)$.

(i) Each basal plane dislocation reacts with two prismatic plane dislocations. Let $\mathbf{b}(1)=\frac{1}{3}a[11\bar{2}0]$ and $\mathbf{n}(1)=(0001)$.

If $\mathbf{b}(2)=\frac{1}{3}a[1\bar{2}10]$ and $\mathbf{n}(2)=(10\bar{1}0)$ then $\mathbf{b}(12)=\frac{1}{3}a[2\bar{1}\bar{1}0]$ and $\mathbf{n}(12)=(0001)$; and if $\mathbf{b}(2)=\frac{1}{3}a[\bar{2}110]$ and $\mathbf{n}(2)=(0\bar{1}10)$ then $\mathbf{b}(12)=\frac{1}{3}a[\bar{1}2\bar{1}0]$ and $\mathbf{n}(12)=(0001)$.

The dislocation P_0Q_0 is therefore glissile in the basal plane and if $\mathbf{b}(1)$ has all six possible values there will be twelve reactions of this type.

(ii) Each basal plane dislocation reacts with four pyramidal plane dislocations. Let $\mathbf{b}(1)=\frac{1}{3}a[11\bar{2}0]$ and $\mathbf{n}(1)=(0001)$.

If $\mathbf{b}(2)=\frac{1}{3}a[1\bar{2}10]$ and $\mathbf{n}(2)=(10\bar{1}1)$ then $\mathbf{b}(12)=\frac{1}{3}a[2\bar{1}\bar{1}0]$ and $\mathbf{n}(12)=(0001)$;

if $(\mathbf{b}2)=\frac{1}{3}a[1\bar{2}10]$ and $\mathbf{n}(2)=(10\bar{1}\bar{1})$ then $\mathbf{b}(12)=\frac{1}{3}a[2\bar{1}\bar{1}0]$ and $\mathbf{n}(12)=(0001)$;

if $\mathbf{b}(2)=\frac{1}{3}a[\bar{2}110]$ and $\mathbf{n}(2)=(01\bar{1}1)$ then $\mathbf{b}(12)=\frac{1}{3}a[\bar{1}2\bar{1}0]$ and $\mathbf{n}(12)=(0001)$;

and if $\mathbf{b}(2)=\frac{1}{3}a[\bar{2}110]$ and $\mathbf{n}(2)=(01\bar{1}\bar{1})$ then $\mathbf{b}(12)=\frac{1}{3}a[\bar{1}2\bar{1}0]$ and $\mathbf{n}(12)=(0001)$.

The dislocation P_0Q_0 is therefore glissile in the basal plane and if $\mathbf{b}(1)$ has all six possible values there will be twenty-four reactions of this type.

(iii) Each prismatic plane dislocation reacts with two other prismatic plane dislocations. Let $\mathbf{b}(1)=\frac{1}{3}a[11\bar{2}0]$ and $\mathbf{n}(1)=(1\bar{1}00)$.

If $\mathbf{b}(2)=\frac{1}{3}a[1\bar{2}10]$ and $\mathbf{n}(2)=(10\bar{1}0)$ then $\mathbf{b}(12)=\frac{1}{3}a[2\bar{1}\bar{1}0]$ and $\mathbf{n}(12)=(01\bar{1}0)$;

and if $\mathbf{b}(2)=\frac{1}{3}a[\bar{2}110]$ and $\mathbf{n}(2)=(0\bar{1}10)$ then $\mathbf{b}(12)=\frac{1}{3}a[\bar{1}2\bar{1}0]$ and $\mathbf{n}(12)=(10\bar{1}0)$.

Downloaded from rsta.royalsocietypublishing.org

The dislocation P_0Q_0 is therefore glissile in a prismatic plane and if the dislocation A_1A_1' has each of the six possible pairs of values of $\mathbf{b}(1)$ and $\mathbf{n}(1)$ there will be six reactions of this type.

(iv) Each prismatic plane dislocation reacts with four pyramidal plane dislocations. Let $\mathbf{b}(1) = \frac{1}{3}a[11\bar{2}0]$ and $\mathbf{n}(1) = (1\bar{1}00)$.

If $\mathbf{b}(2) = \frac{1}{3}a[1\bar{2}10]$ and $\mathbf{n}(2) = (10\bar{1}1)$ then $\mathbf{b}(12) = \frac{1}{3}a[2\bar{1}\bar{1}0]$ and $\mathbf{n}(12) = (0\bar{1}1\bar{1})$;

if $\mathbf{b}(2) = \frac{1}{3}a[1\bar{2}10]$ and $\mathbf{n}(2) = (10\bar{1}\bar{1})$ then $\mathbf{b}(12) = \frac{1}{3}a[2\bar{1}\bar{1}0]$ and $\mathbf{n}(12) = (0\bar{1}11)$;

if $\mathbf{b}(2) = \frac{1}{3}a[\bar{2}110]$ and $\mathbf{n}(2) = (0\bar{1}11)$ then $\mathbf{b}(12) = \frac{1}{3}a[\bar{1}2\bar{1}0]$ and $\mathbf{n}(12) = (10\bar{1}\bar{1})$;

if $\mathbf{b}(2) = \frac{1}{3}a[\bar{2}110]$ and $\mathbf{n}(2) = (0\bar{1}1\bar{1})$ then $\mathbf{b}(12) = \frac{1}{3}a[\bar{1}2\bar{1}0]$ and $\mathbf{n}(12) = (10\bar{1}1)$.

The dislocation P_0Q_0 is therefore glissile in a pyramidal plane and if $\mathbf{b}(1)$ has all six possible values there will be twenty-four reactions of this type.

(v) Each pyramidal plane dislocation interacts with four other pyramidal plane dislocations. Let $\mathbf{b}(1) = \frac{1}{3}a[11\bar{2}0]$ and $\mathbf{n}(1) = (10\bar{1}1)$.

If $\mathbf{b}(2) = \frac{1}{3}a[1\bar{2}10]$ and $\mathbf{n}(2) = (10\bar{1}1)$ then $\mathbf{b}(12) = \frac{1}{3}a[2\bar{1}\bar{1}0]$ and $\mathbf{n}(12) = (01\bar{1}0)$;

if $\mathbf{b}(2) = \frac{1}{3}a[1\bar{2}10]$ and $\mathbf{n}(2) = (10\bar{1}\bar{1})$ then $\mathbf{b}(12) = \frac{1}{3}a[2\bar{1}\bar{1}0]$ and $\mathbf{n}(12) = (01\bar{1}\bar{2})$;

if $\mathbf{b}(2) = \frac{1}{3}a[\bar{2}110]$ and $\mathbf{n}(2) = (0\bar{1}11)$ then $\mathbf{b}(12) = \frac{1}{3}a[\bar{1}2\bar{1}0]$ and $\mathbf{n}(12) = (10\bar{1}0)$;

and if $\mathbf{b}(2) = \frac{1}{3}a[\bar{2}110]$ and $\mathbf{n}(2) = (0\bar{1}1\bar{1})$ then $\mathbf{b}(12) = \frac{1}{3}a[\bar{1}2\bar{1}0]$ and $\mathbf{n}(12) = (10\bar{1}2)$.

In the first and third of these reactions the dislocation P_0Q_0 is glissile in a prismatic plane, but in the second and fourth the slip plane $\mathbf{n}(12)$ is not one which is observed and P_0Q_0 will be sessile. If the dislocation A_1A_1' has each of the twelve possible pairs of values of $\mathbf{b}(1)$ and $\mathbf{n}(1)$ there will be twelve sessile and twelve glissile reactions of this type.

For the hexagonal system there are thus ninety possible attractive reactions of which twelve are sessile and seventy-eight are glissile.

(c) *Body-centred cubic*

Slip directions in this system are of the form $\frac{1}{2}a\langle 111\rangle$. There are three distinct types of reaction which can be classified without regard to the slip planes. If $\mathbf{b}(1)$ is chosen there are four values of $\mathbf{b}(2)$ for which repulsion occurs, three values for which attraction occurs and one case of annihilation. For the attractive junction the Burgers vector of P_0Q_0 is of the form $a\langle 100\rangle$. This slip direction is not observed and all the reactions may be considered as sessile. If the predominant slip planes are {110}, {112} and {123} the set of attractive junctions can be divided into six sets containing respectively 108 {112}{112} reactions, 216 {112}{110} reactions, 96 {110}{110} reactions and 432 of each of the {112}{123}, {110}{123} and {123}{123} reactions: a total of 1716 possible attractive reactions all of which are sessile.

2. Behaviour under stress

When stress is applied to the crystal the dislocation segments will move and change their shape. If elastic anisotropy and the dependence of the line energy on the dislocation orientation are neglected it can be shown that the variation of the free energy is zero when the component dislocations are circular arcs (figure 2). In addition, two transversality

Downloaded from rsta.royalsocietypublishing.org

conditions must be satisfied which are equivalent to the equilibrium of the dislocation arcs meeting at P and Q They are

$$E_1 \cos\psi_1 + E_2 \cos\psi_2 = E_{12} \cos\psi_3 \tag{4}$$

for the P node and a similar one for the Q node; here the ψ angles are the inclinations of the tangents to the dislocation arcs with respect to PQ. These equations describe the motion of the nodes along the line of intersection of the slip planes of the dislocations. The motion will depend on the resolved shear stresses on the active dislocations and on the geometry of

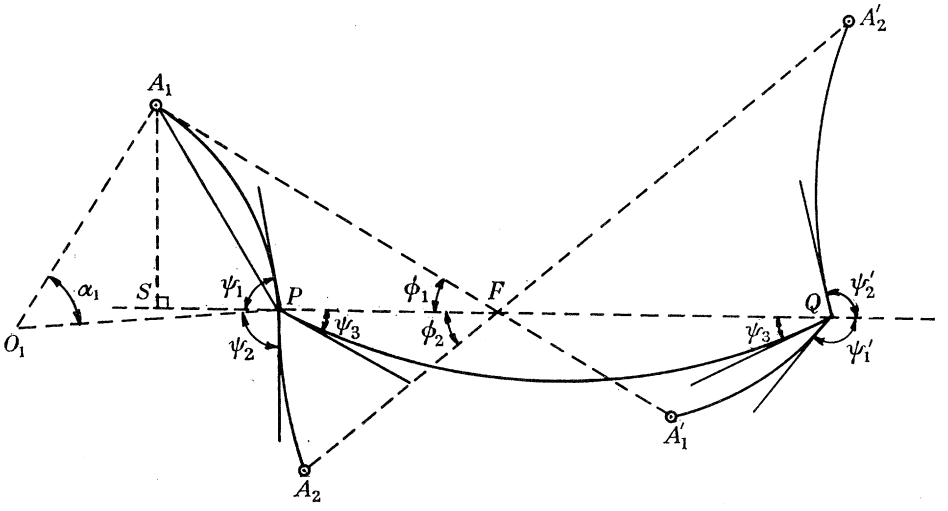

FIGURE 2. The dislocation configuration when stress is applied to the crystal.

the configuration before the attractive reaction occurs. This dependence is complicated and no attempt is made here to give a complete and rigorous description of it. Instead some particular examples are considered in detail and it is thought that these are sufficient to illustrate the important features of the model.

To solve the equations (4) it is necessary to rewrite them in terms of the resolved shear stresses and the co-ordinates of P and Q. It is convenient to introduce some parameters defined as follows. Put $A_1F \equiv \zeta_1 R$, $A_1'F \equiv \zeta_1' R$, $A_2F \equiv \zeta_2 R$, $A_2'F \equiv \zeta_2' R$, $\mathbf{FP} = \epsilon_P R.\mathbf{l}(12)$, $\mathbf{FQ} = \epsilon_Q R.\mathbf{l}_{12}$. The length R is a measure of the size of the configuration and usually the ζ's are taken to be small integers. If σ is an applied tension to the crystal the curvature ρ of a particular glissile dislocation will be proportional to $\beta\sigma$ where β is the normal resolved shear stress factor; i.e. $\rho = |\mathbf{b}|\beta\sigma/E$. The cosine terms in equation (4) can be simply derived with reference to figure 2. If O_1 is the centre of curvature of A_1P and if $\angle A_1OP = \alpha$, then the following simple relations hold:

$$|A_1P|^2 = R^2(\zeta_1^2 + 2\epsilon_P\zeta_1\cos\phi_1 + \epsilon_P^2) = (4/\rho_1^2)\sin^2\frac{\alpha_1}{2}$$

and $$|SP| = |SF| - |PF|, \quad \text{i.e.} \quad \cot(\psi_1 - \tfrac{1}{2}\alpha_1) = \cot\phi_1 + (\epsilon_P/\zeta_1)\operatorname{cosec}\phi_1$$

whence

$$\cos\psi_1 = -\tfrac{1}{2}\rho_1\zeta_1 R\sin\phi_1 \pm (\epsilon_P + \zeta_1\cos\phi_1)\,[(\zeta_1^2 + 2\zeta_1\epsilon_P\cos\phi_1 + \epsilon_P^2)^{-1} - \tfrac{1}{4}\rho_1^2R^2]^{\frac{1}{2}}. \tag{5}$$

The negative sign before the second term occurs when the arc A_1P is greater than a semicircle and when it is zero the arc is a semicircle. In the same way similar expressions can

Downloaded from rsta.royalsocietypublishing.org

be obtained for $\cos\psi_2$, $\cos\psi_1'$ and $\cos\psi_2'$. The $\cos\psi_3$ term can also be simply derived and is given by

$$\cos\psi_3 = [1-\tfrac{1}{4}\rho_3^2R^2(\epsilon_Q-\epsilon_P)^2]^{\frac{1}{2}}. \tag{6}$$

If we use the approximation that $E \simeq \frac{1}{2}G|\mathbf{b}|^2$ (Cottrell 1953) then in the h.c.p. and f.c.c. reactions $E_1 = E_2 = E_{12}$ and in the b.c.c. reactions $E_1 = E_2 = \frac{3}{4}E_{12}$. It is convenient to introduce a dimensionless parameter $\gamma \equiv \sigma R/Gb$, so that the curvature of a glissile dislocation can be written as; $\rho = 2\beta\gamma/R$. Then substituting (5) and (6) in equation (4) gives the relation

$$\begin{aligned} f_1(\epsilon_P,\epsilon_Q,\gamma) \equiv{}& (-\zeta_1\beta_1\sin\phi_1+\zeta_2\beta_2\sin\phi_2)\gamma \\ &+(\epsilon_P+\zeta_1\cos\phi_1)\,[(\zeta_1^2+2\epsilon_P\zeta_1\cos\phi_1+\epsilon_P^2)^{-1}-\beta_1^2\gamma^2]^{\frac{1}{2}}-A[1-\{\beta_3\gamma(\epsilon_Q-\epsilon_P)\}^2]^{\frac{1}{2}} \\ &+(\epsilon_P+\zeta_2\cos\phi_2)\,[(\zeta_2^2+2\epsilon_P\zeta_2\cos\phi_2+\epsilon_P^2)^{-1}-\beta_2^2\gamma^2]^{\frac{1}{2}} = 0 \end{aligned}$$

and

$$\begin{aligned} f_2(\epsilon_P,\epsilon_Q,\gamma) \equiv{}& (-\zeta_1'\beta_1\sin\phi_1+\zeta_2'\beta_2\sin\phi_2)\gamma \\ &+(\epsilon_Q-\zeta_1'\cos\phi_1)\,[(\zeta_1'^2-2\epsilon_Q\zeta_1'\cos\phi_1+\epsilon_Q^2)^{-1}-\beta_1^2\gamma^2]^{\frac{1}{2}}+A[1-\{\beta_3\gamma(\epsilon_Q-\epsilon_P)\}^2]^{\frac{1}{2}} \\ &+(\epsilon_Q-\zeta_2'\cos\phi_2)\,[(\zeta_2'^2-2\epsilon_Q\zeta_2'\cos\phi_2+\epsilon_Q^2)^{-1}-\beta_2^2\gamma^2]^{\frac{1}{2}} = 0. \end{aligned} \tag{7}$$

Here $A = 1$ for f.c.c. and h.c.p. reactions and $A = \frac{4}{3}$ for b.c.c. reactions. Solutions of these equations are of the form

$$\gamma = \gamma(\epsilon_P) \quad \text{and} \quad \gamma = \gamma(\epsilon_Q).$$

For dislocation arcs which are extremals (in this problem they are circular arcs) the free energy is a function of ϵ_P, ϵ_Q, and γ, i.e. $G(\epsilon_P,\epsilon_Q,\gamma)$ and $\partial G/\partial\epsilon_P \equiv f_1$ and $\partial G/\partial\epsilon_Q \equiv f_2$. The conditions for G to be a minimum for a given γ are that

$$\frac{\partial^2 G}{\partial\epsilon_P^2},\ \frac{\partial^2 G}{\partial\epsilon_Q^2} \quad \text{and} \quad \frac{\partial^2 G}{\partial\epsilon_P^2}\frac{\partial^2 G}{\partial\epsilon_Q^2}-\left(\frac{\partial^2 G}{\partial\epsilon_P\,\partial\epsilon_Q}\right)^2,$$

which is equal to the Jacobian $\left|\dfrac{\partial(f_1,f_2)}{\partial(\epsilon_P,\epsilon_Q)}\right|$, are all greater than zero. It can easily be shown that when $\gamma = 0$ this condition is satisfied. If the Jacobian is zero, $\dfrac{\mathrm{d}\gamma}{\mathrm{d}\epsilon_P} = \dfrac{\mathrm{d}\gamma}{\mathrm{d}\epsilon_Q} = 0$. In the special case when f_1 is independent of ϵ_Q and f_2 is independent of ϵ_P, e.g. sessile junctions, only one of these derivatives need be zero. While the sign of the Jacobian is positive neither the sign of $\partial^2G/\partial\epsilon_P^2$ or $\partial^2G/\partial\epsilon_Q^2$ can change and these therefore remain positive at least along the arcs of the $\gamma(\epsilon)$ curves from P_0 or Q_0 to the nearest turning points. The free energy is therefore a minimum for these arcs but when the turning points are passed it is no longer a minimum, though it is not necessarily a maximum.

Inspecting equations (7) it is seen that the solutions depend on a large number of parameters: $3\beta\beta$, $2\phi\phi$, A and $4\zeta\zeta$. To solve the equations for all combinations of these is obviously prohibitive. The most drastic changes in behaviour occur when ϕ_1 and ϕ_2 are varied, for, as will be shown, when they are small the values of γ at the turning points of the $\gamma(\epsilon)$ curves become very large. The effects of changing the resolved shear stresses are less important and some extreme cases are considered here.

Saada (1960*a*) has considered the solutions of equations (7) for a particular set of parameters. In this notation his case corresponds to $\beta_2 = \beta_3 = 0$, $\zeta_1 = \zeta_1' = 2$, $\zeta_2 = \zeta_2' = 1$ and $A = 1$. This particular stress system in f.c.c. crystals gives anomalously large values of γ for small values of ϕ_1 and ϕ_2. However, this stress system is useful since solutions of (7) can be obtained in a simple analytical form; see appendix (A); and it has been used to investigate the effects of varying the ζ's.

PHILOSOPHICAL TRANSACTIONS OF THE ROYAL SOCIETY A MATHEMATICAL, PHYSICAL & ENGINEERING SCIENCES
PHILOSOPHICAL TRANSACTIONS OF THE ROYAL SOCIETY A MATHEMATICAL, PHYSICAL & ENGINEERING SCIENCES

Downloaded from rsta.royalsocietypublishing.org

To investigate the effects of changing the resolved shear stresses β on the behaviour of sessile junctions two extreme cases are considered. In one they are equal in magnitude, i.e. $\beta_1 = \pm\beta_2$, and these reactions are called symmetrical. In the other, one is zero, i.e. β_1 or $\beta_2 = 0$, and these reactions are called asymmetrical. Only one set of ζ parameters is considered. To reduce the number of calculations they are all taken to be equal and, for

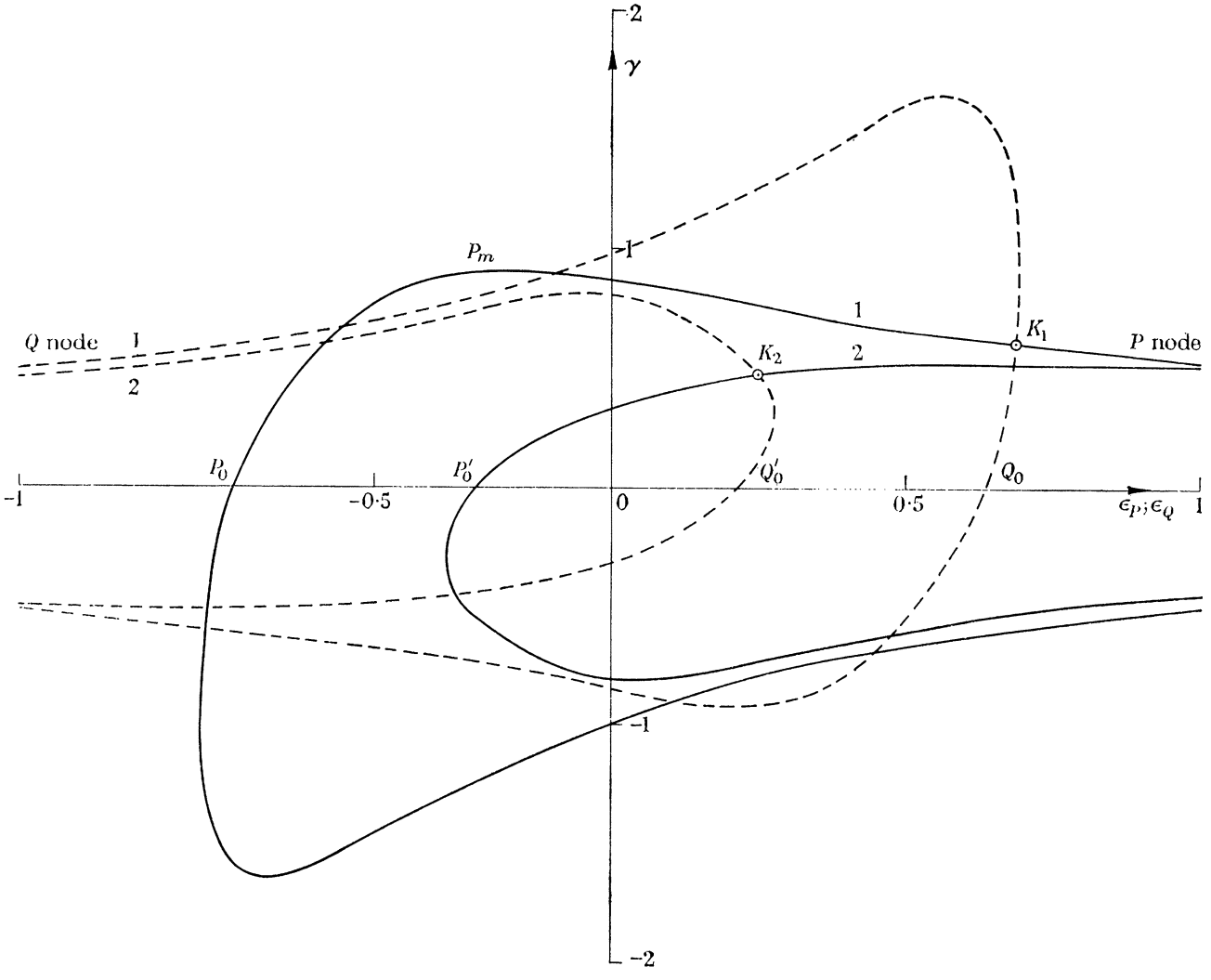

FIGURE 3. The salient features of the curves relating the stress parameter and the node co-ordinate ϵ for sessile junctions.

convenience, equal to one. The reduction in the number of calculations arises from the resulting symmetry properties of equation (7). Thus

$$f_1(\epsilon_P, \epsilon_Q, \gamma) = -f_2(-\epsilon_Q, -\epsilon_P, -\gamma) \tag{8}$$

and this relation is shown in figure 3 where the two $\gamma(\epsilon)$ curves are shown superimposed on the same plane. These curves are typical of the great majority of those calculated for sessile junctions and they show the general features of the behaviour of the junctions as the stress is increased. If the stress parameter 'γ' is increased in the positive sense the node P moves from P_0 to the right, as shown by the full line and in this case Q, shown by the dashed line, initially also moves to the right. If the turning point $P_{m(\max.)}$ on the $\gamma(\epsilon_P)$ curve is to the left

Downloaded from rsta.royalsocietypublishing.org

of the intersection of the P and Q curves then for all points on the arc P_0P_m the P node is in equilibrium. On the other side of P_m, i.e. for all points on the arc P_mK_1, the P node is not in equilibrium and if the stress is increased beyond γ_m this node moves to the right and meets the Q node. The dislocation configuration has then collapsed and the two segments A_1A_1' and A_2A_2' may pass through each other. In figures 4, 5 and 7 these configurations are denoted by dots. Alternatively (curves P_0', Q_0'; figure 3) the turning point may occur to the right of K_2; the nodes will then meet without the configuration collapsing when $\gamma = \gamma_K$ and again the two dislocation segments may subsequently pass through each other. In figures 4, 5 and 7 these configurations are denoted by crosses. The stress γ_f to destroy the configuration is then taken to be either γ_m or γ_K depending whether P_m is to the left or the right of K. From the symmetry relation (8) it is evident that if a particular feature on the $\gamma(\epsilon_P)$ curve occurs at a particular γ value, e.g. γ_m then there will be a similar feature on the $\gamma(\epsilon_Q)$ curve at $\gamma = -\gamma_m$. It is therefore evident that each physical feature is associated with two values of γ, of the same magnitude but opposite sign, and that only one value (positive) need be considered.

(a) *Symmetrically stressed sessile junctions*

For these junctions $\beta_1 = \beta_2 = \beta$, $\beta_3 = 0$ and γ_f has the symmetry relations

$$\gamma_f(\phi_1, \phi_2) = \gamma_f(-\phi_1, -\phi_2) = \gamma_f(\phi_2, \phi_1) = \gamma_f(-\phi_2, -\phi_1). \tag{9}$$

So in calculating the roots of equation (7) only the range of ϕ values defined by the inequalities; $\cos\phi_1 + \cos\phi_2 \geqslant A$ and $\phi_2 \geqslant |\phi_1|$ need be considered. In order to calculate γ_f values of γ were calculated from equation (A 1) for values of ϵ_P in the range -1 to $+1$ at intervals of 0·1 and for values of ϕ_1 and ϕ_2 at 10° intervals. These values, together with contours of equal γ_f, are shown in figure 4. For a particular set of β and ζ parameters the behaviour of the junctions can be described by a single number, representing the average value of γ_f for all values of ϕ_1 and ϕ_2 for which reactions can occur. This average does not however allow for the probability that junctions for which ϕ_1 and ϕ_2 are small are not very likely. The most likely way in which the junctions may be formed would be when dislocations from a comparatively strain-free part of the crystal intersect and become entangled in a forest of dislocations. If the forest dislocation segments are straight they may be described by a distribution function representing the proportion having their lengths, and their inclinations to a particular direction, lying in given ranges. It is reasonable to assume that the length and angular distributions are independent. The intersecting dislocations can be similarly described so that the probability of forming junctions where the lengths A_1F, $A_1'F$, A_2F and $A_2'F$ (figure 1) have particular values will be proportional either to $|\sin\phi_1|$ or $|\sin\phi_2|$, depending on the stress system. The appropriate average stress will then be the weighted average $\langle\beta\gamma_f|\sin\phi_1|\rangle$ and (because of the behaviour of γ_f at small values of ϕ_1 and ϕ_2) it will be considerably smaller than $\langle\gamma_f\rangle$. The choice of integration range used in calculating these averages will be discussed in the second part. These averages are simply defined by the relations

$$\langle\gamma_f\rangle = \frac{\iint_{(A)} \gamma_f \,\mathrm{d}\phi_1\,\mathrm{d}\phi_2}{\iint_{(A)} \mathrm{d}\phi_1\,\mathrm{d}\phi_2} \quad \text{and} \quad \langle\gamma_f|\sin\phi_1|\rangle = \frac{\iint_{(A)} \gamma_f|\sin\phi_1|\,\mathrm{d}\phi_1\,\mathrm{d}\phi_2}{\iint_{(A)} |\sin\phi_1|\,\mathrm{d}\phi_1\,\mathrm{d}\phi_2},$$

Downloaded from rsta.royalsocietypublishing.org

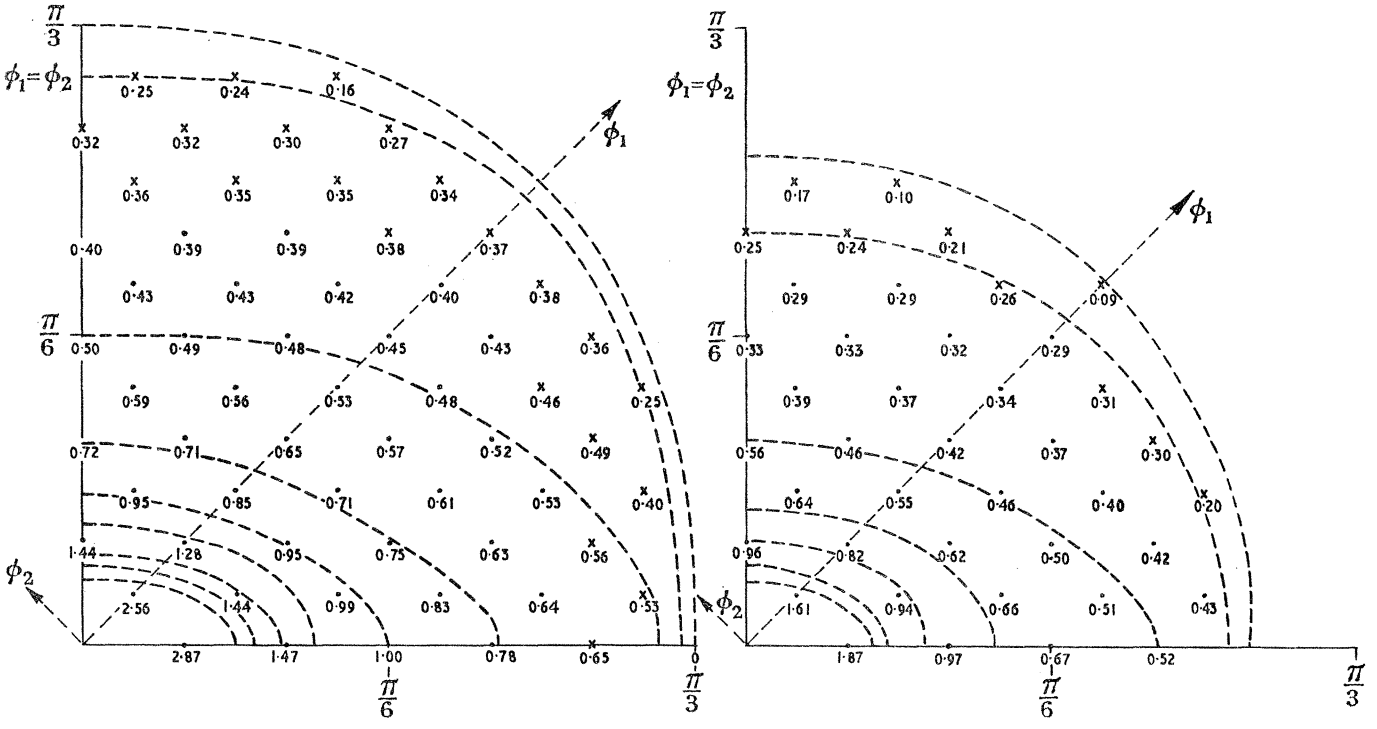

(*a*) f.c.c. ($A = 1$) (*b*) b.c.c. ($A = \frac{4}{3}$)

FIGURE 4. Breaking stresses for sessile junctions with equally stressed components ($\beta_1 = \beta_2 = \beta$; $\beta_3 = 0$).

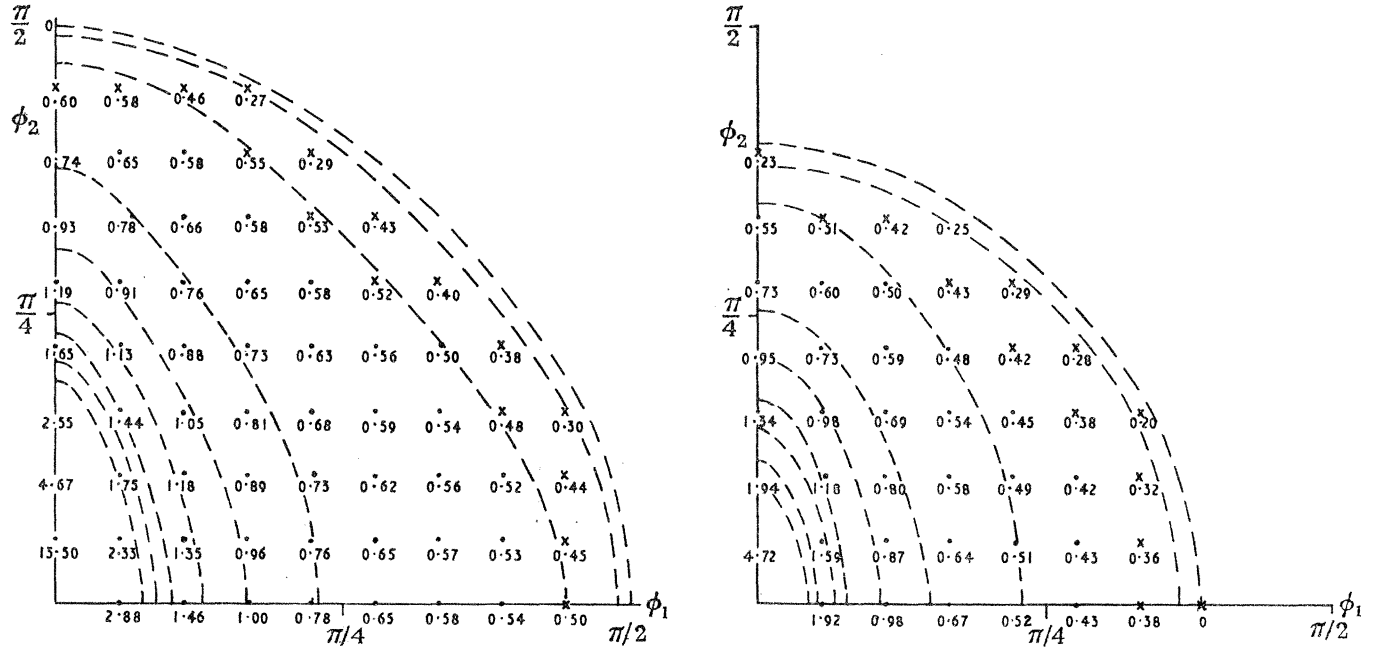

(*a*) f.c.c. ($A = 1$) (*b*) b.c.c. ($A = \frac{4}{3}$)

FIGURE 5. Breaking stresses for sessile junctions with unequally stressed components ($\beta_1 = \beta$; $\beta_2 = \beta_3 = 0$).

where the range of integration (A) is either the whole range of ϕ_1 and ϕ_2 values or it is determined by the inequality (2).

It is shown in appendix A that γ_f has a singularity at $\phi_1 = \phi_2 = 0$. The evalutation of $\langle \beta \gamma_f \rangle$ is divided into two parts; the region around the singularity gives a contribution equal

Downloaded from rsta.royalsocietypublishing.org

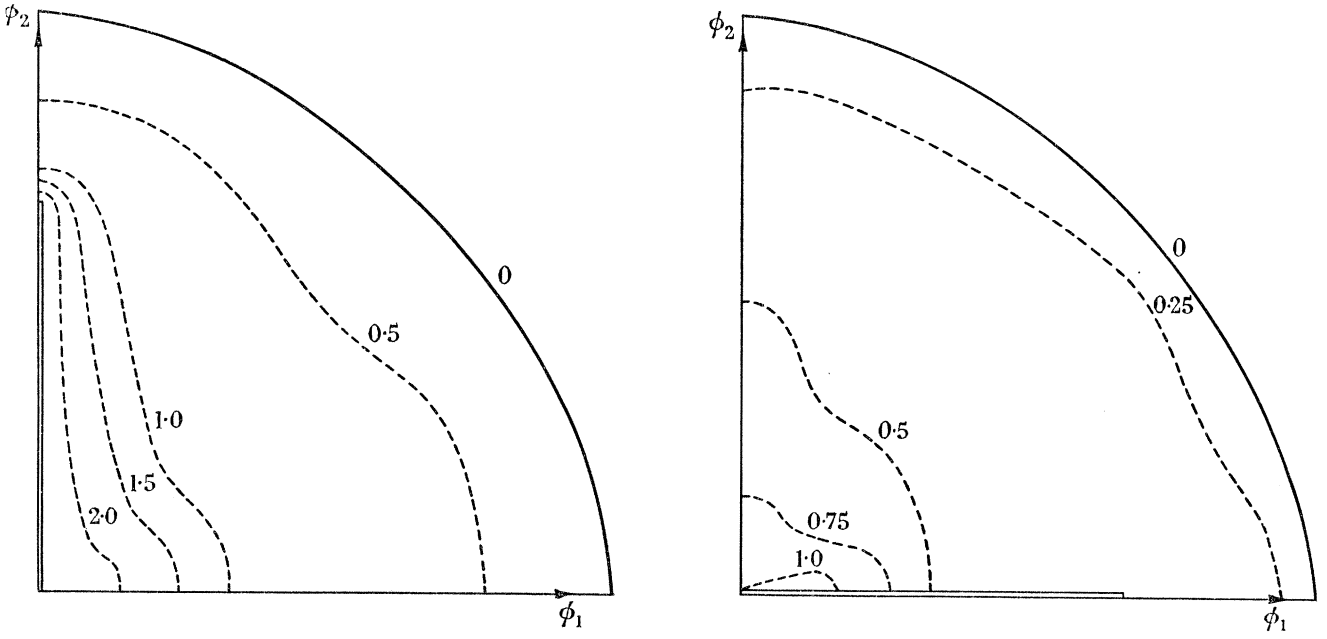

(*a*) $\zeta_1 = 1, \zeta_2 = 2$ (*b*) $\zeta_1 = 2, \zeta_2 = 1$

FIGURE 6. γ_f contours for junctions formed from dislocations of unequal lengths.

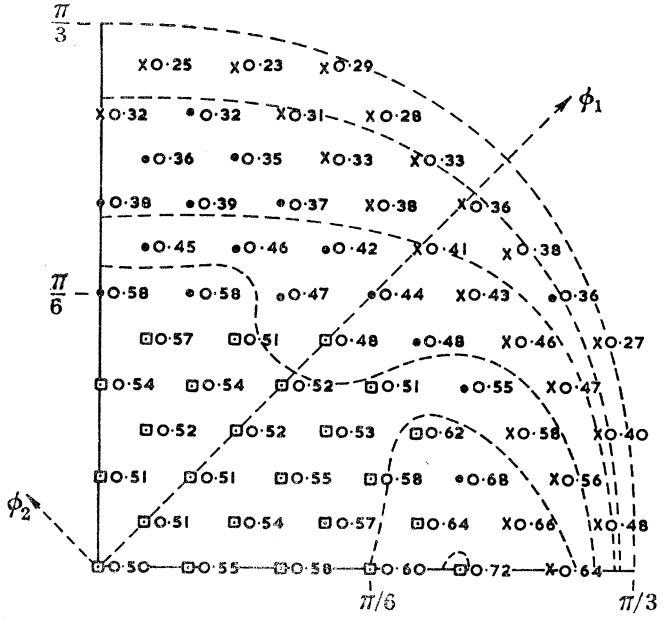

FIGURE 7. Breaking stresses for a glissile junction with equally stressed components ($A = 1$; $\beta_1 = \beta_2 = \beta_3 = 1$).

to $0{\cdot}601\,(2-A)$; and the contribution from the remainder is calculated to be 3·96 for $A = 1$ and 1·99 for $A = \frac{4}{3}$. The total numerators are thus 4·56 and 2·39 respectively. For the whole range of ϕ values the denominator is π^2 so that $\langle \beta\gamma_f \rangle = 0{\cdot}462$ and 0·242 respectively. For the other range, defined by the inequality (2), the denominators are 7·28 and 5·85 so that $\langle \beta\gamma_f \rangle = 0{\cdot}626$ when $A = 1$ and $\langle \beta\gamma_f \rangle = 0{\cdot}518$ when $A = \frac{4}{3}$.

The alternative weighted average can be calculated in a similar way (appendix A). For this stress system $\langle \beta\gamma_f | \sin\phi_1 | \rangle = \langle \beta\gamma_f | \sin\phi_2 | \rangle$. The contribution to the numerator from the

Downloaded from rsta.royalsocietypublishing.org

singularity region is much smaller in this case: $0{\cdot}0186\,(2-A)$: and the total numerators are 1·92 for $A = 1$ and 0·964 for $A = \frac{4}{3}$. The denominator for all possible junctions is 2π and the weighted averages are 0·306 and 0·153 respectively. If only those junctions which are formed are considered the numerators are 3·988 and 2·349 and the weighted averages are 0·476 when $A = 1$ and 0·405 when $A = \frac{4}{3}$.

These averages are all summarized in table 1.

TABLE 1. AVERAGE BREAKING STRESSES

		average breaking stress for attractive junctions formed			average breaking stress for all attractive junctions		
crystal symmetry	stress system	$\langle\beta\gamma_f\rangle$	$\langle\beta\gamma_f\lvert\sin\phi_1\rvert\rangle$	$\langle\beta\gamma_f\lvert\sin\phi_2\rvert\rangle$	$\langle\beta\gamma_f\rangle$	$\langle\beta\gamma_f\lvert\sin\phi_1\rvert\rangle$	$\langle\beta\gamma_f\lvert\sin\phi_2\rvert\rangle$
f.c.c. and h.c.p., $A = 1$	$\beta_1 = \beta_2 = \beta;\ \beta_3 = 0$	0·626	0·476	0·476	0·462	0·192	0·192
	$\beta_1 = 0,\ \beta_2 = \beta;\ \beta_3 = 0$	0·959	0·609	0·737	0·707	0·243	0·298
	$\beta_1 = \beta;\ \beta_2 = \beta_3 = 0$	0·959	0·737	0·609	0·707	0·298	0·243
	$\beta_1 = \beta_2 = \beta_3 = \beta$	0·440	0·414	0·414	0·324	0·167	0·167
b.c.c., $A = \frac{4}{3}$	$\beta_1 = \beta_2 = \beta;\ \beta_3 = 0$	0·518	0·405	0·405	0·242	0·0963	0·0963
	$\beta_1 = 0,\ \beta_2 = \beta;\ \beta_3 = 0$	0·752	0·501	0·401	0·352	0·119	0·0955
	$\beta_1 = \beta;\ \beta_2 = \beta_3 = 0$	0·752	0·401	0·501	0·352	0·0955	0·119

(*b*) *Asymmetrically stressed sessile junctions*

For these junctions $\beta_2 = \beta_3 = 0$ and γ_f has the symmetry relations

$$\gamma_f(\phi_1, \phi_2) = \gamma_f(-\phi_1, \phi_2) = \gamma_f(\phi_1, -\phi_2) = \gamma_f(-\phi_1, -\phi_2). \tag{10}$$

In this case the roots of equation (7) need only be calculated for the range of ϕ values defined by the inequalities $\cos\phi_1 + \cos\phi_2 \geqslant A$ and $\phi_1, \phi_2 \geqslant 0$. The values of γ_f obtained are shown in figure 5 and it is evident that contours of γ_f for the two values of A are quite different. The detailed analysis given in appendix B shows that for $A = \frac{4}{3}$, γ_f is proportional to ϕ_1^{-1} when $\phi_2 = 0$ and to ϕ_2^{-1} when $\phi_1 = 0$. This is similar to the behaviour of the symmetrically stressed junctions but when $A = 1$, γ_f is proportional to ϕ_1^{-1} when $\phi_2 = 0$ but to $\phi_2^{-\frac{3}{2}}$ when $\phi_1 = 0$. This behaviour makes calculation of the averages a little more difficult. However, what is more important, their values are anomalously large.

There are simple relations between the average weighted stresses when either the A_1A_1' or the A_2A_2' dislocation is unstressed:

$$\left.\begin{aligned}\langle\gamma_f\lvert\sin\phi_1\rvert\rangle_{\beta_2=0} &= \langle\gamma_f\lvert\sin\phi_2\rvert\rangle_{\beta_1=0}\\ \langle\gamma_f\lvert\sin\phi_2\rvert\rangle_{\beta_2=0} &= \langle\gamma_f\lvert\sin\phi_1\rvert\rangle_{\beta_1=0}\end{aligned}\right\} \quad (\beta_1 = \beta_2).$$

For $A = \frac{4}{3}$ the calculation of the averages was similar to that used for the symmetrically stressed junctions. They are outlined in appendix B and the results are shown in table 1. For $A = 1$ the calculation is somewhat more difficult; see appendix B; because of the peculiar behaviour of γ_m near the singularity at $\phi_1 = \phi_2 = 0$. This is to some extent eliminated in the weighted averages and the difference between $A = 1$ and $A = \frac{4}{3}$ is much less than the corresponding difference in the averages (see table 1).

(*c*) *Junctions with unequal arms*

It is shown in appendix B that for asymmetrically stressed sessile junctions a simple analytical description of the behaviour can be given when A_1A_1' and A_2A_2' are unequal but

Downloaded from rsta.royalsocietypublishing.org

still bisected at F (figure 1). The unequal arms introduce discontinuities in the variation of γ_m as a function of ϕ_1 and ϕ_2. Referring to figure 1, if for simplicity we consider $A = 1$ then if $\phi_1 = 0$, A_2P_0 is normal to P_0Q_0 since in equation (3) $\psi_{10} = \phi_1 = 0$ and $E_1 = E_2 = E_{12}$ so that $\cos\psi_{20} = 0$. If $|A_1F| < |A_2F|$ the point P should lie to the left of P_0. This configuration is not possible since the dislocation line tensions at P would act only along the directions PF and PA_2 and cannot therefore be in equilibrium. In appendix B it is shown analytically that this is equivalent to the first equation of (7) having no real root. No real roots are possible for any value of ϕ_2 for which $|A_1F| < |A_2F|\cos\phi_2$ and this range represents a discontinuity in the junction behaviour which is marked by the double line along the ϕ_2 axis shown in figure 6 (*a*). However, if ϕ_1 is not exactly zero real roots exist and the junctions behave in the normal way when the stress is increased. This discontinuous behaviour occurs solely as a consequence of assuming that the ends of the dislocation A_2A_2' are immovable points. The behaviour also means that some of the average breaking stresses already discussed cannot be calculated. The contours of constant breaking stress for cases when $|A_1F|$ is less than and greater than $|A_2F|$ are shown respectively in figures 6 (*a*) and (*b*); the latter case corresponds to the model discussed by Saada. In case (*a*) the averages $\langle\beta_1\gamma_f\rangle$ and $\langle\beta_1\gamma_f|\sin\phi_2|\rangle$ are infinite but $\langle\beta_1\gamma_f|\sin\phi_1|\rangle$ can be calculated and it is approximately 0·24. $\langle\beta_1\gamma_f|\sin\phi_1|\rangle$ for case (*b*) was found to be approximately 0·20: the same as Saada's value when expressed in this notation. If the stressed segment becomes infinitely long this weighted average tends to zero but if the unstressed segment does likewise the weighted average is approximately 0·80. It should be emphasized that these discontinuities will occur for all stress systems.

(*d*) *Glissile junctions*

In the sessile junctions each of the average breaking stresses is a function of the ratio of the resolved shear stresses β_1/β_2. For a glissile junction, where there is another β parameter, the average breaking stresses will be a function of two variables. In addition to this feature the behaviour of individual junctions is somewhat more complicated and at small angles the motion of the nodes is quite different. A complete calculation of the behaviour of these junctions would therefore be prohibitively long, but that given here is thought to demonstrate the main features. In order to study the effects of the angular and stress parameters on their behaviour it was thought sufficient to examine the variation of γ_f as a function of ϕ_1 and ϕ_2 for a particular stress system, and then, for some particular values of ϕ_1 and ϕ_2, to examine the effects of changing the stress on the glissile segment P_0Q_0. To avoid the difficulties encountered when either one of the dislocations, A_1A_1' or A_2A_2', is unstressed or when the arms are unequal, the stress system is chosen to be: $\beta_1 = \beta_2$; β_3 with $\zeta_1 = \zeta_1' = \zeta_2 = \zeta_2' = 1$. For this type of junction the symmetry relations (9) still apply. The solutions of the equations (7) for the particular stress-system $\beta_1 = \beta_2 = \beta_3$ were obtained by an iterative calculation based on the 'regula-falsi' method for the solution of simultaneous non-linear equations. Curves of $\gamma_P(\epsilon)$ and $\gamma_Q(\epsilon)$ were obtained by solving the equations to obtain ϵ_P and ϵ_Q for values of γ at intervals of 0·2 in the range $0 < \gamma < 2$. The appropriate values of γ_f were then obtained numerically, as for the sessile junctions, and the contours of equal γ_f are shown in figure 7. These contours are not complicated and since there are no singularities the averages can be readily calculated and are shown in table 1. However the

Downloaded from rsta.royalsocietypublishing.org

values of γ_f for small values of ϕ_1 and ϕ_2, though they refer to turning points in the $\gamma(\epsilon)$ curves, do not represent breaking stresses as described for the sessile junctions. These configurations are denoted by squares. This feature is more clearly seen in the behaviour of the junctions as β_3 is varied.

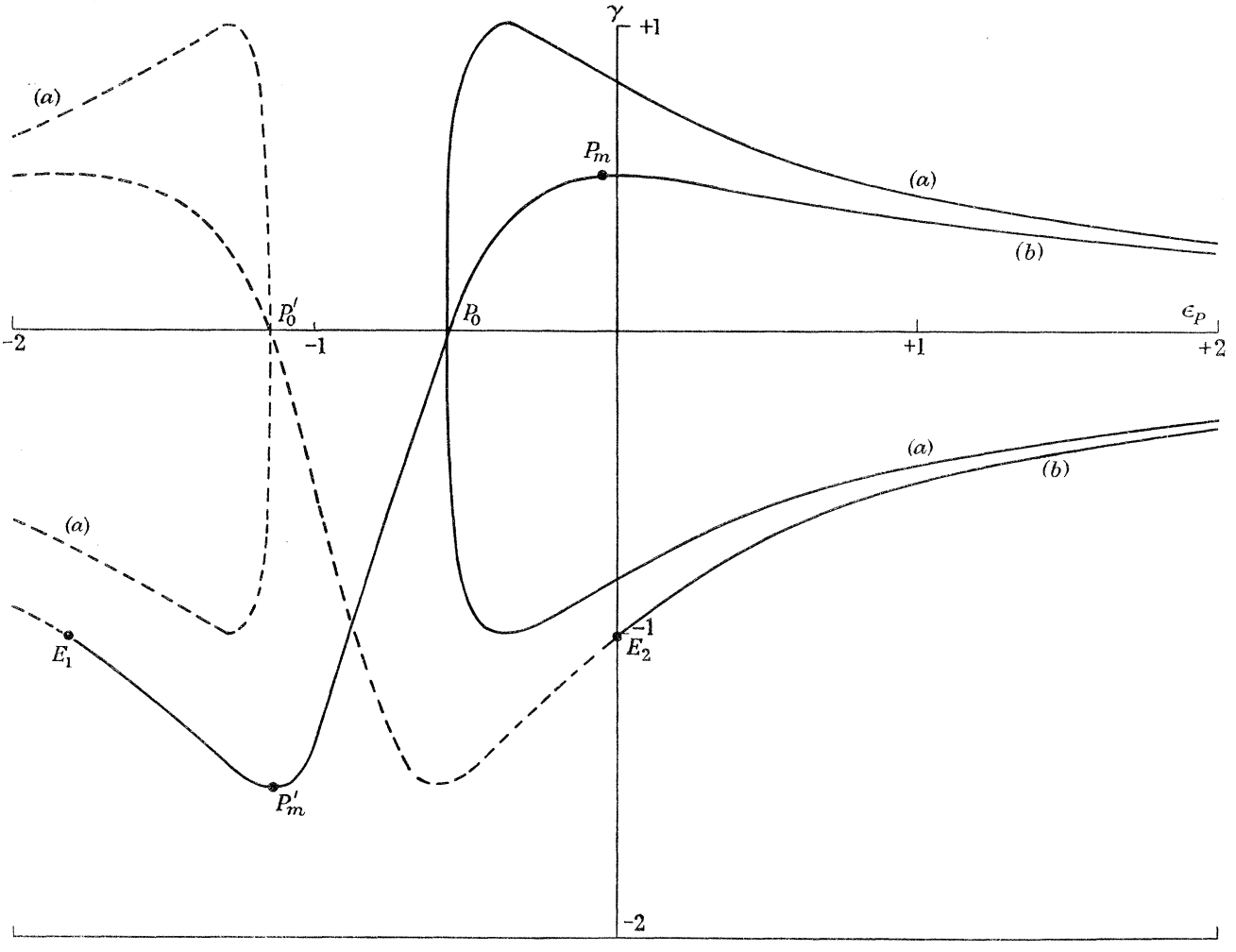

FIGURE 8. Possible forms of the curve relating the stress parameter γ and the node co-ordinate ϵ for sessile junctions.

It is possible too to obtain simple analytical solutions for these glissile junctions when $\phi_1 = -\phi_2 = \phi$ (see appendix C). In this appendix it is shown that there are four types o solution which are illustrated in figure 9 (a), (b), (c), (d). In these diagrams the thick curves represent solutions that can be realized from zero stress: the thin lines represent other mathematically possible solutions. It is also shown in appendix C that the reactions considered in this paper the dislocation configurations represented by the isolated arcs (thin lines) are unstable. In case (a) the stress on the junction dislocation and the angle ϕ are large; in case (d) only the latter is large. As the stress on the crystal is increased the nodes come together and the configuration eventually breaks down in the way described for the sessile junctions. For small values of ϕ the behaviour is shown in diagrams (b) and (c). In (b) the junction stress is large and in (c) it is small. In these cases the nodes diverge as the stress is increased up to a maximum. If the stress is maintained or increased the nodes

Downloaded from rsta.royalsocietypublishing.org

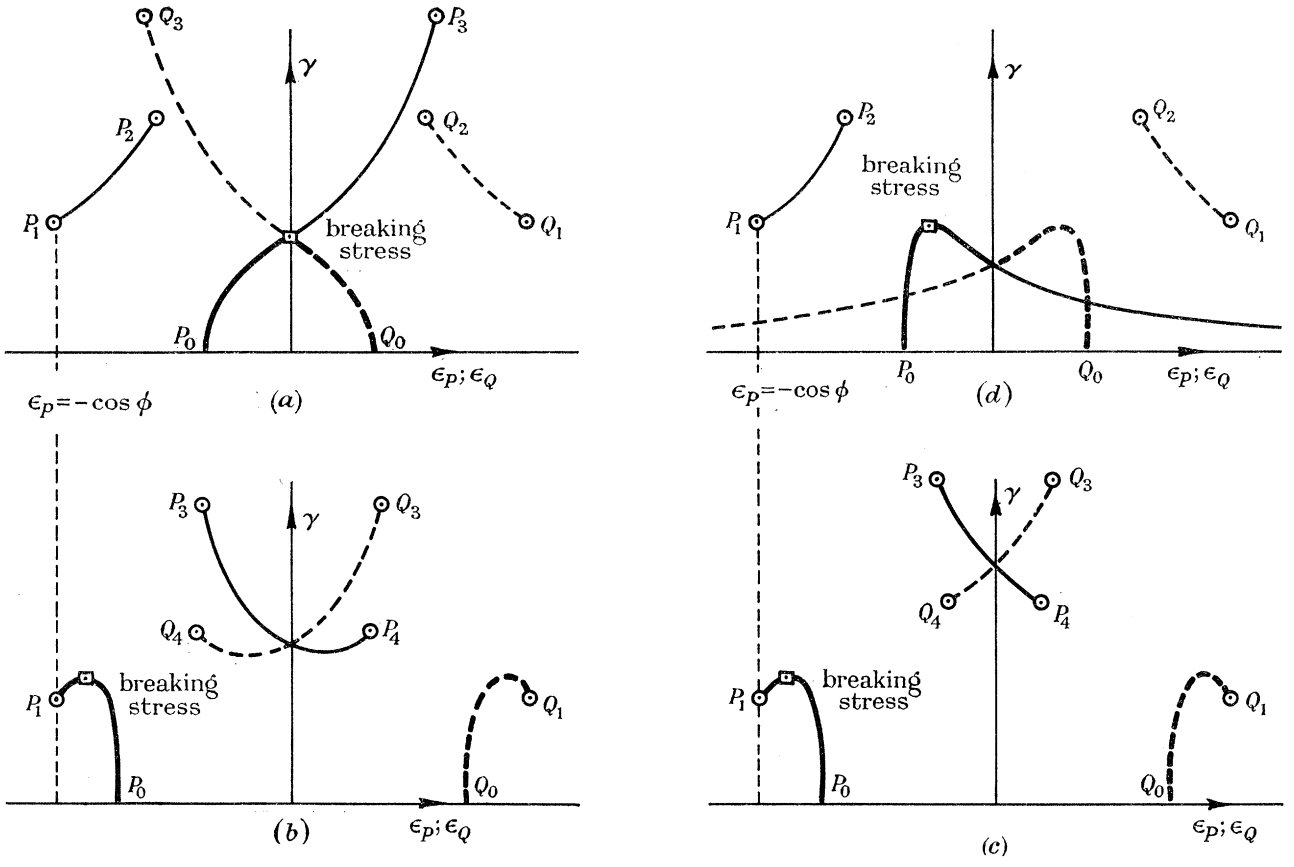

FIGURE 9. Possible forms of the curves $\gamma = \gamma(\epsilon)$ for a symmetrically stressed f.c.c. glissile junction with $\phi_1 = -\phi_2 = \phi$.

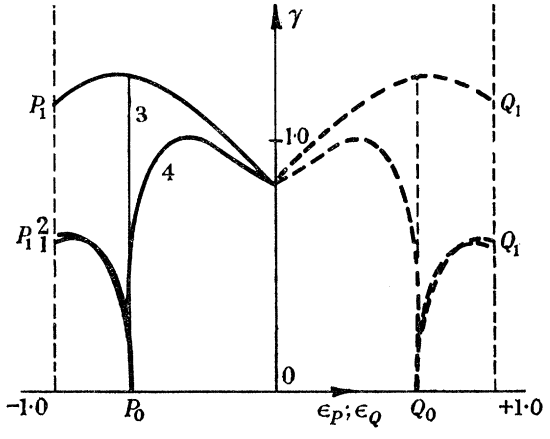

FIGURE 10. (*a*) The behaviour of glissile junctions as the stress on the glissile arc is changed. $A = 1$. $\phi_1 = \phi_2 = 30°$. Four stress systems showing behaviour of both nodes:

1, $\beta_1 = \beta_2 = 0$; $\beta_3 = 1$.
2, $\beta_1 = \beta_2 = 1$; $\beta_3 = 1$.
3, $\beta_1 = \beta_2 = 1$; $\beta_3 = \frac{1}{2}$.
4, $\beta_1 = \beta_2 = 1$; $\beta_3 = 0$, i.e. sessile.

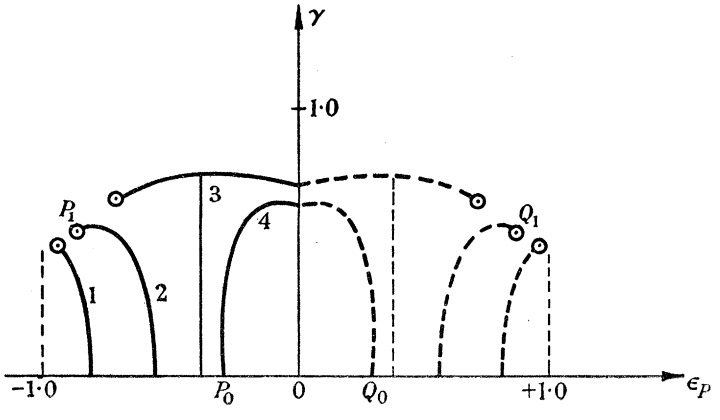

(*b*) The behaviour of glissile junctions as the intersection angle is changed. $A = 1$. $\beta_1 = \beta_2 = \beta_3 = 1$. $\phi_1 = \phi_2 = \phi$.

1, $\phi = 15°$. 2, $\phi = 30°$.
3, $\phi = \arctan \frac{1}{2}\sqrt{3}$. 4, $\phi = 45°$.

Downloaded from rsta.royalsocietypublishing.org

continue to diverge, the structure becomes unstable and begins to undergo complex changes of configuration at the points P_1 and Q_1. When these points are reached the junction dislocation is semicircular and can spread freely until it meets some other part of the configuration and further junctions can form.

To show the effect of changing the ratio $m = \beta_3/\beta_1$ for a fixed ϕ, curves were calculated for some special values of $|m|$. These are shown in figure 10 (*a*) (in which the physically possible solutions only are recorded). Curve 3 is a critical case where the dislocation nodes do not move at all until the maximum stress is reached, after which the configuration may collapse by either of the alternative modes. Similar curves are shown in figure 10 (*b*) indicating the behaviour when ϕ is changed while $|m|$ is fixed. As $\phi \to 0$ the arc P_0P_1 becomes a straight line through $\epsilon_P = -1$ and parallel to the γ axis. If $\phi_1 = -\phi_2$ the limiting value of γ is equal to $\frac{1}{2}$. For large values of ϕ the γ_f values are close to those for the symmetrically stressed face-centred cubic sessile junctions. This is to be expected, since the influence of the glissile arc is decreased with increasing intersection angle ϕ_1 and ϕ_2.

II. APPLICATION OF RESULTS TO WORK HARDENING

The structure in which the forest intersection mechanism is most likely to be important, and to which the present calculations are particularly designed to apply, is that found for example in polycrystalline metals of medium or high-stacking fault energy after more than a few per cent strain. Here most of the dislocations are arranged in irregular tangles or cell walls with a considerably lower dislocation density in the intervening spaces (see, for example, Hirsch 1959*a*; Keh & Weissmann 1963). It will be assumed that the forest contribution to the flow stress in such a structure is the stress required to force an isolated dislocation through some region in the structure within which the dislocation density can be taken as substantially uniform. This contribution will be estimated first for a purely random type of dislocation forest, e.g. the initial Frank network existing in the annealed crystal. The possibility of forming non-random dislocation tangles on straining will then be considered and the forest contribution from these structures will be examined.

To estimate the probable importance of the forest mechanism it is necessary first to compare the magnitudes of the predicted flow stresses due to different types of forest with the observed flow stresses of metals at known dislocation densities. However, since the magnitude of the forest contribution cannot be calculated with sufficient accuracy, it is not possible to decide on the importance of this mechanism solely on this basis. The predicted characteristics of work hardening by the forest intersection mechanism will therefore be compared with the observed characteristics of work hardening in various metals to obtain further evidence on this point.

3. Flow-stress contribution from a random forest

In a random forest it will be assumed that the forest dislocations pierce the active glide planes at random angles, and that the distribution of their Burgers vectors is also random. It is then necessary to calculate the flow-stress contribution from such a forest in terms of the mean spacing l of forest dislocations of all types, i.e. the spacing that is measured experimentally.

Downloaded from rsta.royalsocietypublishing.org

Three types of interaction must be considered for any given glissile dislocation:

(*a*) The long-range interaction with trees forming attractive intersections, as discussed in the calculations of part I.

(*b*) The long-range interaction with trees forming repulsive intersections.

(*c*) The short-range interaction to form jogs on the intersecting dislocations as they separate.

The (*a*) and (*b*) interactions are long range only in so far as they extend over distances that are too large to allow thermal fluctuations to be of assistance in overcoming them Saada (1960*b*). Much longer range forces can arise from certain dislocation arrays such as pile-ups.

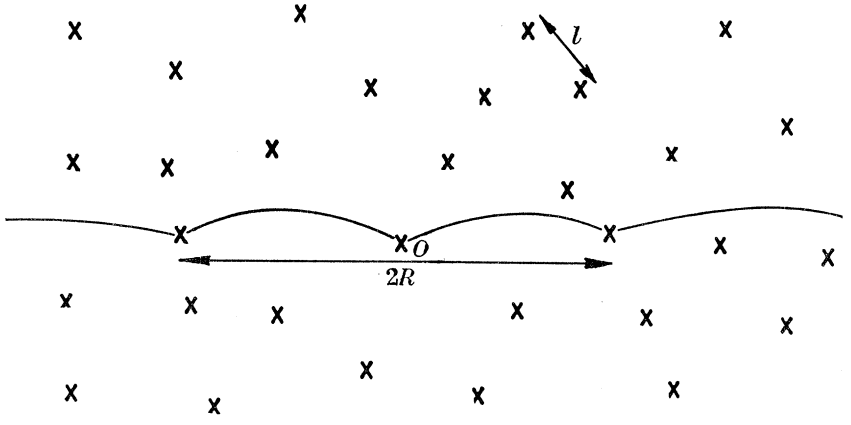

FIGURE 11. Glissile dislocation moving over slip lane intersected by forest dislocations, showing the difference between mean pinning distance R on either side of obstacle O, and mean forest spacing, l.

At low temperatures all three types of interaction must be considered, but above some critical temperature T_c, thermal activation will overcome the short-range interactions (*c*) and only (*a*) and (*b*) will be important.

The resolved shear stress τ on a glissile dislocation required to make it overcome an obstacle of a given type is of the form (Cottrell 1953)

$$\tau = \alpha(Gb/R),$$

where α is a coefficient indicating the strength of the obstacle and R is the mean distance on either side of the obstacle at which the moving dislocation is pinned at the instant the obstacle is overcome (figure 11). R will be proportional to the mean forest spacing. If $R = nl$, where l is the mean forest spacing, then both α and n must be known for each type of obstacle in order to compute the total forest contribution to the flow stress. Values of α and n for the types of interaction listed above will now be estimated.

(*a*) *Attractive intersections*

For attractive intersections, values of the coefficient α for junctions of different types and different angular configurations are given by the values of $\beta\gamma_f$ in the contour diagrams of figures 4 to 7 since $\tau = \beta\gamma_f(Gb/R)$. The flow-stress contribution from a forest of attractive trees has been calculated by Saada (1960*b*), Friedel (1959) and Carrington *et al.* (1960) using average values of the function $\beta\gamma_f$ such as those shown in table 1. However, an average

Downloaded from rsta.royalsocietypublishing.org

value for all junctions has no precise physical significance. For example, very weak junctions will be broken at stresses below the applied stress and hence cannot contribute to the total flow stress of the crystal. A more rigorous analysis of the problem is therefore required.

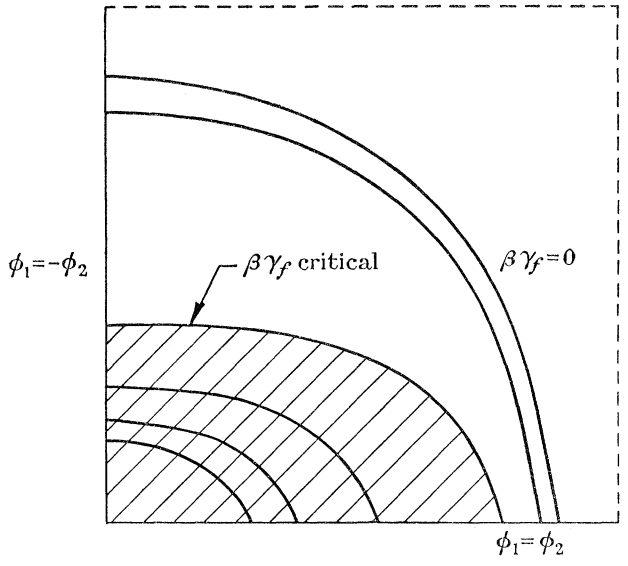

FIGURE 12. Schematic contour diagram showing breaking stresses of attractive intersections of one type but different angular parameters ϕ_1 and ϕ_2. At any applied stress τ_1 junctions outside the contour $\beta\gamma_f = Gb/R\tau$ will be broken and those inside the area (shown hatched) will be unbroken.

Consider first a uniformly spaced dislocation forest, composed solely of trees forming a given type of attractive junction with a particular glissile dislocation. We shall examine the stress required to force this glissile dislocation through such a forest. The breaking stresses of junctions of one type but of different angular configuration can be represented by a contour diagram, as shown schematically in figure 12 (i.e. as in figures 4 to 7). As the stress τ on the glissile dislocation is raised from zero, an increasing number of junctions—those lying outside some critical $\beta\gamma_f$ contour—will be broken, so that the trees still forming effective obstacles will become less dense and so more widely spaced. The parameter R is thus a variable, being inversely proportional to the square root of the density of junctions remaining unbroken at any given applied stress. Using the weighting factor $\sin\phi_2$ for the probability of an intersection with a forest dislocation lying at an angle ϕ_2 (as defined in figure 1), the relation between R and the spacing R_0 of junctions stable at zero stress is

$$R = pR_0, \quad \text{where} \quad p = \left\{ \frac{\int_{(A_2)} |\sin\phi_1| \, \mathrm{d}\phi_1 \, \mathrm{d}\phi_2}{\int_{(A_1)} |\sin\phi_1| \, \mathrm{d}\phi_1 \, \mathrm{d}\phi_2} \right\}^{\frac{1}{2}}. \tag{11}$$

Here A_1 is the area bounded by the critical $\beta\gamma_f$ contour (shown hatched in figure 12) and A_2 is the area bounded by $\beta\gamma_f = 0$. Hence since

$$\tau = \beta\gamma_f (Gb/R),$$

we have

$$\tau R_0/Gb = \beta\gamma_f/p.$$

Downloaded from rsta.royalsocietypublishing.org

Plots of $\tau R_0/Gb$ against $\beta\gamma_f$ for different types of junctions are shown in figure 13 (a), the values of p being obtained by numerical integration from the calculated contour diagrams shown in figures 4 to 7. As the $\beta\gamma_f$ value is increased from zero, the increased strength of the remaining obstacles at first outweighs the decrease in their density, and the applied

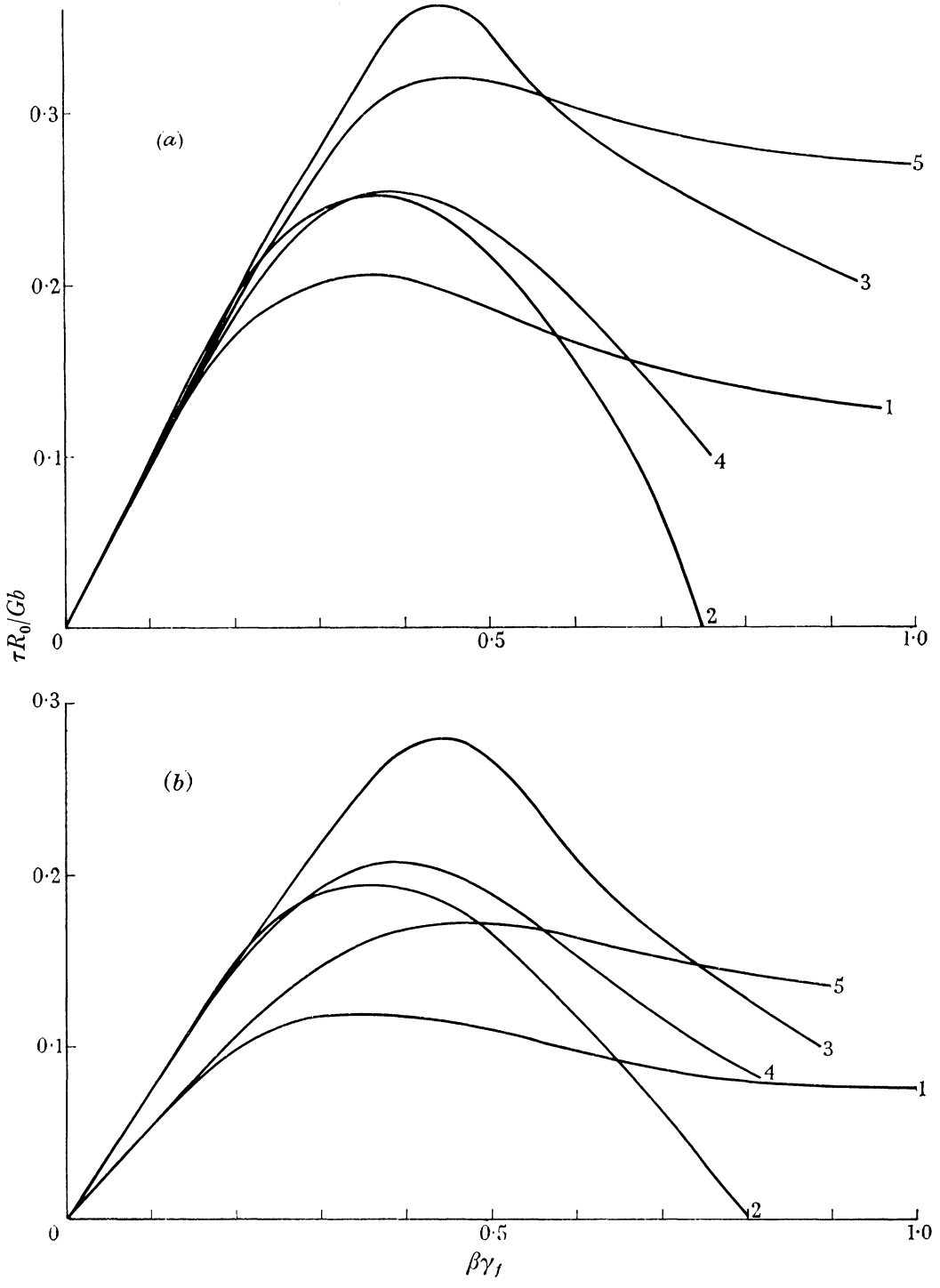

FIGURE 13. Applied stress τ on a glissile junction as a function of breaking stress $\beta\gamma_f$ of junctions in terms of (a) spacing R_0 of forest dislocations forming attractive intersections, and (b) spacing R_0' of all forest dislocations with suitable Burgers vectors for forming attractive intersections. 1, b.c.c. ($s.$); 2, f.c.c. ($g.$); 3, f.c.c. (a); 4, f.c.c. ($s.$); 5, b.c.c. ($a.$).

PHILOSOPHICAL TRANSACTIONS OF THE ROYAL SOCIETY A MATHEMATICAL, PHYSICAL & ENGINEERING SCIENCES
PHILOSOPHICAL TRANSACTIONS OF THE ROYAL SOCIETY A MATHEMATICAL, PHYSICAL & ENGINEERING SCIENCES

Downloaded from rsta.royalsocietypublishing.org

stress τ increases. However as the contour is moved inwards a stage is reached where the weakening due to the increase in spacing of the remaining junctions balances the increase in their strength. This stage corresponds to the calculated maxima in $\tau R_0/Gb$ and these maxima must represent the limiting resistances of these types of forest to the passage of a glissile dislocation. The values of $\tau_{\max.} R_0/Gb$ obtained in this way are shown in table 2. The function $\tau R_0'/Gb$ is plotted against $\beta\gamma_f$ in figure 13 (b), R_0' being the spacing of all forest intersections lying within the range $0 \leqslant |\phi_1, \phi_2| \leqslant \frac{1}{2}\pi$, i.e. the spacing of all forest dislocations of a particular Burgers vector, independent of whether or not they are able to form junction dislocations with the glissile dislocation at zero stress. This range of ϕ_1 and ϕ_2 values will define the new area A_2 in equation (11). The values of $\tau_{\max.} R_0'/Gb$ obtained from these curves (table 2) represent more accurately the resistances of purely random types of dislocation forest to the passage of a glissile dislocation, and they will be used in subsequent discussions of this type of forest.

TABLE 2. RESISTANCES OF VARIOUS TYPES OF FOREST TO THE PASSAGE OF A GLISSILE DISLOCATION

(Long-range interaction stress only.)

	type of attractive intersection formed and assumed stress system	limiting resistance for attractive junctions formed $\frac{\tau_{\max.} R_0}{Gb}$		limiting resistance for all attractive junctions $\frac{\tau_{\max.} R_0'}{Gb}$	
f.c.c.	(1) sessile $\beta_1 = \beta; \beta_2 = \beta_3 = 0$	0·36		0·28	
	(2) sessile $\beta_1 = \beta_2 = \beta; \beta_3 = 0$	0·25	0·29	0·21	0·23
	(3) glissile $\beta_1 = \beta_2 = \beta_3 = \beta$	0·25		0·19	
b.c.c.	(1) sessile $\beta_1 = \beta_2 = \beta; \beta_3 = 0$	0·21	0·26	0·12	0·15
	(2) sessile $\beta_1 = \beta; \beta_2 = \beta_3 = 0$	0·32		0·17	

Comparison of these values with the weighted averages in columns 2, 3, 5 and 6 of table 1 shows appreciable differences, especially in the case where only the junctions formed are considered.

Mott (1952) and Friedel (1959, 1964) have pointed out that it is inaccurate to equate the spacing of obstacles in a slip plane with the spacing of such obstacles along a dislocation moving over the slip plane. If the obstacles are weak they will be unable to deflect the dislocation line greatly, and intersections will be widely spaced (figure 14 (a)). It is only if the obstacles are strong (figure 14 (b)) that the spacing of intersections will approach the spacing of obstacles. However, using the relation between the two spacings derived by Friedel (1963) it can be shown that for comparatively strong junctions in the region of the $\beta\gamma_f$ contours corresponding to $\tau_{\max.}$ values, the error involved in equating the two spacings is not serious within the accuracy of the present estimations (say $\pm 50\%$). It is largely counterbalanced if one equates the resolved shear stress τ on the glissile dislocation to the maximum shear stress $\frac{1}{2}\sigma$ on the crystal under a uniaxial tensile stress σ, i.e. $\beta = \frac{1}{2}$. This latter approximation will therefore be used in comparing observed and calculated flow stresses.

Downloaded from rsta.royalsocietypublishing.org

The values of $\tau_{\max.} R'_0/Gb$ collected in table 2 can now be used to estimate the contribution τ_a of attractive intersections to the forest flow stress in different lattices. For f.c.c. metals cases (1) and (2) in table 2 represent primarily cases where the junction dislocation is a Lomer–Cottrell sessile, but they also represent fairly accurately cases where the junction dislocation is glissile but under a low resolved shear stress. In any case the values for the

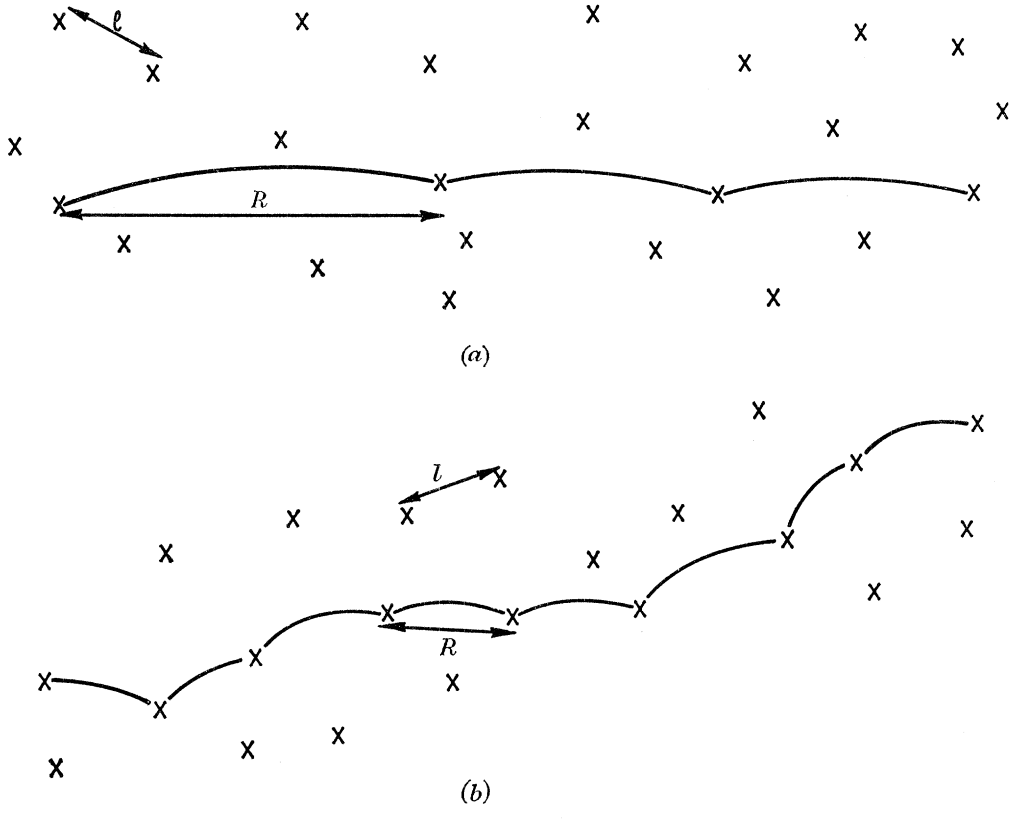

FIGURE 14. Relation between mean intersection spacing, R, and mean obstacle spacing, l, for (a) weak obstacles where $R > l$ and (b) strong obstacles where $R \simeq l$.

different types of junction and stress system are sufficiently close to allow an arithmetic mean to be taken of both sessile and glissile cases without introducing serious error, giving

$$\tau_a \simeq 0{\cdot}23(Gb/R'_0) \tag{12}$$

for f.c.c. metals. As discussed previously, one forest dislocation in three in a random forest should have a Burger's vector suitable for forming attractive intersections with a given glissile dislocation in this structure, so that

$$R'_0 = \sqrt{3}\, l \quad \text{and} \quad \tau_a \simeq 0{\cdot}13(Gb/l),$$

where l is the spacing of forest dislocations of all types.

As discussed earlier, very few intersections in h.c.p. metals could give sessile junction dislocations, but again the possibility exists that the resolved shear stress on the junction dislocation will be low so that it will act as a sessile. In any case the average value of τ_a will be only slightly smaller than for f.c.c. metals, i.e. about $0{\cdot}11\,(Gb/l)$.

Downloaded from rsta.royalsocietypublishing.org

All junction dislocations in b.c.c. metals (which have Burgers vectors of the type $a\langle 100\rangle$) have been assumed to be sessile, but even if this is wrong it appears from the foregoing that no serious error will have been introduced. Since here three out of every eight forest dislocations will have a suitable Burgers vector to form an attractive intersection, $R_0' = \sqrt{\frac{8}{3}}\, l$ and

$$\tau_a \simeq 0{\cdot}15\,(Gb/R_0') \simeq 0{\cdot}09\,(Gb/l). \tag{13}$$

(*b*) *Repulsive intersections*

The stress τ_r required to force a dislocation through a repulsive tree is very difficult to calculate accurately although we know from the argument of Carrington *et al.* (1960) that it must be appreciably smaller than for a corresponding attractive tree. Saada (1960*b*) has estimated that repulsive interactions are 3 to 4 times weaker than attractive ones in f.c.c. crystals, and in the absence of more accurate data this ratio will be assumed to hold for other crystals also. We therefore have

$$\begin{aligned} \tau_r &\simeq 0{\cdot}07\,(Gb/R_0') && \text{for f.c.c. metals,} \\ &\simeq 0{\cdot}04\,(Gb/R_0') && \text{for b.c.c. metals.} \end{aligned}$$

In a random forest, attractive and repulsive trees will be present in roughly equal numbers: the ratios are 6/7, 3/4 and 2/3 for f.c.c., b.c.c. and h.c.p. crystals respectively. At high temperatures where the force for jog formation is negligible, it is clear that the repulsive trees should have little effect since most will be broken before the maximum resistance of the attractive trees is reached. However a few repulsive interactions (those where either the dislocations are nearly parallel of the mean pinning distance R is particularly small) will still be effective obstacles at this stress so that the total long-range flow-stress contribution may be slightly, but hardly significantly, greater than the values of τ_a obtained above.

(*c*) *Formation of jogs*

Below some critical temperature T_c, thermal fluctuations will be unable to supply sufficient energy to form the intersection jogs on two dislocations cutting each other so that additional applied stress will be required (Cottrell 1953). Near 0 °K, all the jog energy will have to be supplied by the applied stress.

The shear stress required to form intersection jogs on unextended dislocations near 0 °K has variously been estimated at

$$\tau_j = (0{\cdot}05 \text{ to } 0{\cdot}2)\, Gb/R,$$

where R is the pinning distance at the instant the jog is formed (see, for example, Friedel 1956; Basinski 1959; Carrington *et al.* 1960).

Saada (1960*b*) has shown that in the case of the intersection of a glissile dislocation with a repulsive 'tree' the jog stress and the long range stress τ_r should be additive, so that near 0 °K the total resistance arising from repulsive interactions should be

$$\begin{aligned} \tau_r + \tau_j &= (0{\cdot}12 \text{ to } 0{\cdot}27)\, Gb/R_0' && \text{for f.c.c. crystals,} \\ &= (0{\cdot}09 \text{ to } 0{\cdot}24)\, Gb/R_0' && \text{for b.c.c. crystals.} \end{aligned}$$

Since the jog stress is present for weak and strong junctions alike it can be added to other stresses when expressed in terms of R_0'.

For attractive intersections the situation is different. First, it has been pointed out (Carrington *et al.* 1960) that as soon as the two dislocations combine to form a junction

Downloaded from rsta.royalsocietypublishing.org

dislocation, they must become half jogged so that only half the jog energy need be supplied when the dislocations finally separate. Secondly, in approximately one half of the junctions in the region of the critical $\beta\gamma_f$ contours, the stress-node position curve is of the type shown in figure 3, curve (1), i.e. maximum stress is reached before the nodes come together so that it is not necessary to add the jog stress to the maximum long-range stress (see also Saada 1960*a*). Jog stresses should thus be less than half the values for repulsive interactions and we may estimate the total resistance from attractive intersections near 0 °K to be

$$\begin{aligned} \tau_a+\tau_j &= (0{\cdot}25 \text{ to } 0{\cdot}33)\, Gb/R_0' \quad \text{for f.c.c. crystals,} \\ &= (0{\cdot}17 \text{ to } 0{\cdot}25)\, Gb/R_0' \quad \text{for b.c.c. crystals.} \end{aligned}$$

Hence if the lower limit is accepted for jog energies, repulsive interactions will remain considerably weaker than attractive ones down to 0 °K, and will therefore contribute little to the total flow stress. This will then be given by

$$\begin{aligned} \tau_{\text{total}} = \tau_a+\tau_j &\simeq 0{\cdot}25\,(Gb/R_0') \simeq 0{\cdot}14\,(Gb/l) \quad \text{for f.c.c. crystals,} \\ &\simeq 0{\cdot}17\,(Gb/R_0') \simeq 0{\cdot}10\,(Gb/l) \quad \text{for b.c.c. crystals.} \end{aligned}$$

However, if the upper limit for τ_j is more accurate, repulsive interactions will become of appreciable importance as the temperature is lowered and result in a considerable increase in flow stress above that calculated from attractive intersections alone. Near 0 °K the density of strong barriers would be doubled with both attractive and repulsive trees forming obstacles of equal strength so that

$$\begin{aligned} \tau_{\text{total}} = \tau_a+\tau_j \simeq \tau_r+\tau_j &\simeq 0{\cdot}30\,(Gb/R_0') \simeq 0{\cdot}30\,(Gb/l) \quad \text{for f.c.c. crystals,} \\ &\simeq 0{\cdot}25\,(Gb/R_0') \simeq 0{\cdot}25\,(Gb/l) \quad \text{for b.c.c. crystals.} \end{aligned}$$

(R_0' is now approximately equal to l, since repulsive intersections can pin a dislocation on either side of an attractive intersection, and vice versa.)

The above final averages are collected together for comparison in table 3.

TABLE 3. TOTAL RESISTANCES OF VARIOUS TYPES OF FOREST TO THE PASSAGE OF A GLISSILE DISLOCATION (APPROXIMATE VALUES)

temperature range	assumed value of $\frac{\tau_j R}{Gb}$	random forest $\frac{\tau R_0'}{Gb}$	random forest $\frac{\tau l}{Gb}$	non-random forest $\frac{\tau l}{Gb}\left(\approx\frac{\tau R_0'}{Gb}\right)$
f.c.c.				
$\geqslant T_c$	0	0·23	0·13	0·26
near 0 °K	0·05	0·25	0·14	0·28
	0·2	0·30	0·30	0·30
b.c.c.				
$\geqslant T_c$	0	0·15	0·09	0·18
near 0 °K	0·05	0·17	0·10	0·20
	0·2	0·25	0·25	0·25

4. THE FLOW-STRESS CONTRIBUTION FROM NON-RANDOM DISLOCATION FORESTS

Although the assumption used above of a random type of dislocation forest may be reasonable for the original Frank network in an annealed crystal, it is unlikely to be accurate for the dislocation tangles or cell walls formed on straining. These are associated with definite misorientations (often alternating in sign) so that each wall cannot consist of purely random

Downloaded from rsta.royalsocietypublishing.org

types of dislocations with positive and negative Burgers vectors occurring with equal frequency.

Since attractive intersections are stronger than repulsive ones (at least at high temperatures where cell formation is pronounced), dislocation tangles or cell walls would be expected to build up in which dislocations from two intersecting slip systems make attractive intersections with each other. Each cell wall of this type should therefore act as a strong barrier to dislocations of say two particular Burgers vectors $\mathbf{b}_1$ and $\mathbf{b}_2$, while allowing those with slip vectors $-\mathbf{b}_1$ and $-\mathbf{b}_2$ together with most of those whose slip vectors lie in different directions, to pass through relatively easily. Where this is the case there will be a tendency to build up a series of cell walls of alternate signs, so that a dislocation passing through one cell will be held up at the next one. The type of cell wall observed in thin foils is therefore to be expected from the characteristics of forest intersections.

In such a structure, surface slip lines extend over distances of many times the mean cell diameter (see, for example, Seeger 1958*b*) so that the forest contribution to the flow stress must be governed by the resistance of the 'strong' cell walls to any given glissile dislocation. The first characteristic of such a 'strong' wall or tangle is that the forest dislocations within it intersecting the glide plane of the glissile dislocation are predominantly of a single Burgers vector, this being such that attractive intersections are formed with the glissile dislocation. We may therefore put R_0' in equations (12) and (13) $\simeq l$ instead of $\sqrt{3}\,l$ or $\sqrt{\frac{8}{3}}\,l$ as in a random forest. The strength of the wall is thus increased by these factors in f.c.c. and b.c.c. crystals respectively. Secondly, the angles of intersection ϕ_1 and ϕ_2 may no longer be purely random as assumed previously since stronger intersections will be preferred. If, for example, the angles were such that all intersections produced junction dislocations (i.e. $\cos\phi_1+\cos\phi_2>1$ in f.c.c. crystals and $\cos\phi_1+\cos\phi_2>\frac{4}{3}$ in b.c.c. crystals) then the resistances would be raised by further factors of *ca.* 30% and *ca.* 80% respectively, as shown by the comparison of values in table 2. It is difficult to estimate the latter effect accurately, but it would seem not unreasonable to conclude that the 'strong' non-random tangles or cell walls produced on straining will be at least twice as strong as a random forest of the same mean spacing l. These estimated values are also shown in table 3. The figures given correspond to cell walls which are twice as strong. Of course the 'weak' cell walls will offer considerably less resistance to the dislocation being considered than an area of random forest of the same spacing.

5. Comparison of forest intersection stress with observed flow stress

Several experimental workers have examined the relation between flow stress and dislocation density in f.c.c. and b.c.c. metals. Their results are expressed satisfactorily by the equation

$$\tau=\tau_0+\alpha Gb\sqrt{\rho},$$

where ρ is the dislocation density and τ_0 and α are constants. For f.c.c. metals the friction stress term τ_0 is usually small enough to be neglected, but it is appreciable in b.c.c. metals. In the text the term 'flow stress' will be used for convenience to describe the part of the flow stress due to strain hardening, i.e. $\tau-\tau_0$. The dislocation density used in the equation may be an average value ρ_a or the density in the cell walls ρ_c. It is usually found that ρ_c is four to five times greater than ρ_a.

Downloaded from rsta.royalsocietypublishing.org

TABLE 4. OBSERVED VALUES α IN EQUATION

$(\tau = \tau_0 + \alpha Gb\sqrt{\rho}.)$

metal or alloy	form	α	source
Ag	polycrystalline	0·55 (ρ_a)	Bailey & Hirsch (1960)
		0·25 (ρ_c)	Bailey & Hirsch (1960)
Ag and Cu	polycrystalline	0·50 (ρ_a)	Bailey (1963)
		0·22 (ρ_c)	Bailey (1963)
Cu-Al alloys	single crystals	0·50 (ρ_a)	Venables (1962)
Ag	single crystals	0·55 (ρ_a)	Levinstein & Robinson (1963)
Fe	polycrystalline	0·4 (ρ_a)	Carrington *et al.* (1960)
Fe	polycrystalline	0·4 (ρ_a)	Keh (1962)
Fe	polycrystalline	0·2 (ρ_c)	Keh (1962)

Experimental values for α are shown in table 4. From these we can take:

$$\tau \simeq 0{\cdot}53\, Gb\sqrt{\rho_a} \simeq 0{\cdot}24\, Gb\sqrt{\rho_c} \qquad \text{for f.c.c. metals,}$$

and

$$\tau \simeq \tau_0 + 0{\cdot}4\, Gb\sqrt{\rho_a} \simeq \tau_0 + 0{\cdot}2\, Gb\sqrt{\rho_c} \qquad \text{for b.c.c. metals.}$$

Since $\sqrt{\rho} = 1/l$ for a particular region, these values of $\tau l/Gb$ can be compared directly with the estimated values of $\tau l/Gb$ in table 3. The experimental measurements were made at room temperature where the jog contribution to the flow stress is small (see, for example, Basinski 1959), so that the relevant values in table 3 should be those obtained from the attractive long range and repulsive intersections alone.

This comparison shows that only the cell walls have a sufficiently high dislocation density to give an appreciable forest contribution to the flow stress (especially since the cell interiors have a dislocation density considerably less than ρ_a). If the cell walls are composed of random arrangements of dislocations then the forest intersection mechanism could account for only about half the observed flow stress, on the basis of the present estimations.

However, non-random dislocation tangles of the type discussed above can account satisfactorily for the total flow stress of a strained metal. Also each cell wall of this type would act as discussed above, i.e. as a selective barrier to dislocations, trapping those with certain Burgers vectors and allowing the others to pass through. Cell walls with definite misorientations should therefore tend to form. This model is thus in satisfactory agreement with the experimental observations discussed so far. However, in view of the uncertainties inherent in some of the approximations that had to be made in arriving at the values in table 3, it is considered insufficient to establish the importance of the forest mechanism on this basis alone. Further comparisons will therefore be made between observed and predicted characteristics of the forest model.

6. CHARACTERISTICS OF FOREST HARDENING

(*a*) *Orientation dependence*

In polycrystals the necessity for coherency to be maintained between the different grains requires that several slip systems should be operative in each grain. There is thus always the opportunity for the forest mechanism to be effective. However, it is possible to stress single crystals so that macroscopic slip takes place on only one slip system or in various combinations of two or more slip systems. If the forest mechanism is important we should then expect to see rapid hardening only when the stress system is such that attractive intersections between dislocations on different glide planes are likely to be frequent.

PHILOSOPHICAL TRANSACTIONS OF THE ROYAL SOCIETY A MATHEMATICAL, PHYSICAL & ENGINEERING SCIENCES

PHILOSOPHICAL TRANSACTIONS OF THE ROYAL SOCIETY A MATHEMATICAL, PHYSICAL & ENGINEERING SCIENCES

Downloaded from rsta.royalsocietypublishing.org

F.c.c. single crystals show this behaviour at low strains. The extent of easy glide (stage 1) is shorter and its slope θ_I greater at orientations of the tensile axis near to the [100], [111] and [110] corners of the unit triangle, and also near the [100]–[111] boundary (see, for example, Clarebrough & Hargreaves 1959). Towards the latter boundary and the [110] corner the highly stressed slip systems should interact to form Lomer–Cottrell sessiles, while towards the [100] and [111] corners both Lomer–Cottrell and glissile intersections should be frequent. The regions of extensive easy glide with a low value of θ_I are near the centre of the triangle and towards the [100]–[110] and [111]–[110] boundaries; these are the orientations where attractive (or repulsive) interactions should be infrequent.

Seeger (1958*b*) has explained these effects on the basis of the curtailment of easy glide by the formation of long Lomer–Cottrell sessiles which act as barriers behind which pile-ups form. Although this mechanism can be used to explain the orientation effects in detail (Clarebrough & Hargreaves 1960) the calculations of part I show that long Lomer–Cottrell barriers, being associated with large values of R, should be relatively weak, collapsing easily by inward movement of the terminal nodes. A curtailment of easy glide by a large number of more closely spaced forest dislocations thus seems more likely. This would be in agreement with the thin foil observations of Steeds, reported by Hirsch (1964).

During stage II and stage III deformation there is very little orientation dependence of work hardening, even although deformation may still be predominantly confined to the primary slip plane. If the forest mechanism is important at this stage, it must be assumed that there is at least localized slip on intersecting systems to produce an increase in forest density. It may be noted that the arguments put forward by Seeger and co-workers (see, for example, Seeger 1958*a*) to show that forest intersections are unimportant at this stage, depend on the assumption that the forest contribution is highly temperature dependent. This may well be wrong, especially if the main barrier to a given type of dislocation is a forest region where it makes predominantly strong attractive intersections. This latter aspect is discussed more fully in the following section.

Few measurements have been made on the orientation dependence of work hardening in b.c.c. single crystals. Jaoul & Gonzalez (1960) reported no difference in the rates of work hardening of iron single crystals oriented for single and duplex slip. Dohi (1959) however reported that single crystals oriented for single slip showed slow linear hardening whereas those in which multiple slip occurred showed more rapid parabolic hardening. The evidence thus seems to be contradictory and further experimental observations are clearly required on this important point. If in fact there is no orientation dependence the forest mechanism is unlikely to be important in b.c.c. crystals.

H.c.p. metals are well known to work harden much more slowly as single crystals, where only basal slip usually takes place, than as polycrystals where other slip systems are forced to act (Elam 1935; Schmid & Boas 1935). Titanium and zirconium are exceptions to this rule, and these deform on many slip systems as single crystals (McQuillan & McQuillan 1956; Rapperport 1955). Forest hardening is thus a possibility for hexagonal metals. A former difficulty in explaining the work hardening of these metals was that practically all intersections produce glissile and not sessile junction dislocations. Since both have been shown here to possess very similar breaking strengths, this difficulty is now removed.

Downloaded from rsta.royalsocietypublishing.org

(*b*) *Temperature and strain rate dependence of flow*

The measurement of the effect of a sudden decrease in temperature or increase in strain rate on the flow stress of a strained metal has been used as a method of distinguishing long-range or temperature insensitive obstacles from short-range or temperature sensitive ones. The original measurements of Cottrell & Stokes (1955) and Adams & Cottrell (1955) on aluminium and copper suggested that the ratio of flow stresses at two given temperatures was independent of strain (the Cottrell–Stokes law). This implied that the long- and short-range forces arose from the same obstacles, so that, although the density of such obstacles rose on straining the ratio of the temperature sensitive part of the flow stress τ_S to the temperature insensitive part τ_G did not change. The only obstacle that could be envisaged which could give rise to both long- and short-range interactions with a glissile dislocation, was a forest dislocation piercing the glide plane at an angle appreciably less than 90° (Basinski 1959; Hirsch 1959*b*); here the elastic interaction would be responsible for τ_G and jog formation on intersection for τ_S.

It has since been pointed out that early measurements showing that τ_S/τ_G was independent of strain had only been carried out at high strains, and that if measurements are made in stages I and II of the deformation of face-centred cubic crystals, a considerably higher ratio of τ_S/τ_G is obtained (Diehl & Berner 1960; Mitra, Osborne & Dorn 1961). This has been used (Mader, Seeger & Thieringer 1964) as an indication that the forest mechanism cannot explain the work hardening behaviour of face-centred cubic single crystals.

No attempt will be made here to predict the ratio of τ_S/τ_G at various temperatures, since it is considered that τ_S and τ_G cannot be estimated with the necessary accuracy.† However, it should be pointed out that with a random type of dislocation forest, such as presumably exists in annealed crystals, the importance of jog formation should be greater than in the types of dislocation tangles or cell walls which it has been shown should form during deformation, in which strong attractive intersections with high τ_G and low τ_S values are likely to play a dominant role. Hence a decrease in the ratio of τ_S/τ_G with increasing strain, such as has been found in f.c.c. single crystals, is not inconsistent with the forest mechanism.

In body-centred cubic metals, no clear indication has been found of a temperature dependent part of the flow stress due to work hardening (Basinski & Christian 1960; Mordike & Haasen 1962; Conrad & Schoeck 1960; Conrad & Frederick 1962). Since the forest mechanism should always show at least a small temperature-dependent contribution due to jog formation, this would tend to discount the importance of forest hardening in b.c.c. metals. However, it is possible that a small jog effect would be masked in b.c.c. metals by the very large temperature dependence of the friction stress.

The temperature and strain rate dependence of flow in single crystals of the hexagonal metal magnesium have been studied by Basinski (1960) and by Conrad, Hays, Schoeck & Wiedersich (1961). Both concluded that the temperature sensitive part of the flow stress was probably due to the formation of jogs during the intersection of primary and forest dislocations, and Basinski also suggested that the temperature insensitive part of the flow

† However, the observed ratio of τ_S/τ_G (e.g. Basinski 1959) is within the range of values predicted from the average flow stresses for different temperatures summarized in table 3 taking $\tau_{0\,°K} = \tau_G + \tau_S$ and $\tau_{(>T_0)} = \tau_G$.

PHILOSOPHICAL TRANSACTIONS OF THE ROYAL SOCIETY A MATHEMATICAL, PHYSICAL & ENGINEERING SCIENCES

PHILOSOPHICAL TRANSACTIONS OF THE ROYAL SOCIETY A MATHEMATICAL, PHYSICAL & ENGINEERING SCIENCES

Downloaded from rsta.royalsocietypublishing.org

stress arose from forest intersections. The sign of the deviation from the Cottrell–Stokes law at low strains was found to be the same as for f.c.c. single crystals suggesting that in this case also there may be a change from a random forest to non-random tangles on straining.

(*c*) *The Bauschinger effect*

Orowan (1959) has shown that the Bauschinger effect can be explained satisfactorily on the forest mechanism of work hardening. Dislocations moving in one direction under a positive stress are assumed to be held up at the edge of a region of dense obstacles, now identifiable as a cell wall. Further movement in this direction will force them into still denser regions. They are held sufficiently by attractive intersections not to move back when the stress is removed, but when the stress is increased in the reverse direction the dislocations will be released and will then be able to move a considerable distance in the reverse direction until they reach the next region where obstacles are dense, i.e. the next cell wall of the same sign. On this theory the Bauschinger effect is thus due more to an increased slip distance for reverse straining than to any internal stresses produced on straining.

(*d*) *The unloading yield point*

A number of workers have observed that when f.c.c. metals (either single or polycrystalline) are strained, unloaded and then immediately reloaded, a sharp yield point is formed. After the yield drop is completed the stress-strain curve returns to that for uninterrupted loading (Haasen & Kelly 1957; Makin 1958; Bolling 1959). This immediate effect must be due to interactions between dislocations during unloading.

The calculations in part I on the behaviour of attractive intersections under stress suggest a possible explanation for this effect. It was shown that where the angles of intersection ϕ_1 and ϕ_2 (figure 1) are low in the case of a sessile intersection, the stress/node curve shows a peak before the two nodes meet and the dislocations separate (curve 1, figure 3). It has been assumed so far that intersection occurs effectively at zero stress so that the nodes ran back to their most stable configurations at P_0 and Q_0 (figure 3). The stress parameter γ must then be increased to $\gamma(P_m)$ to break the intersection. However, if the stress under which the dislocations first meet is less than $\gamma(P_m)$ but greater than $\gamma(\epsilon_P = 0)$ the nodes will not be able to run back to their stable positions at P_0 and Q_0, and the junction will be broken immediately. This effect will give rise to some reduction in the mean strength of attractive intersections, but the amount of this reduction is very difficult to compute. However, it does mean that if the applied stress is removed, a number of attractive intersections will be made within a tangled region which would not have been stable had the dislocations met under stress. The flow stress on reloading should therefore be temporarily increased. This explanation is consistent with the results of Birnbaum (1961) who established the importance of forest intersections in determining the magnitude of the increase in flow stress due to unloading.

No unloading yield point has been observed in magnesium single crystals (Basinski 1960). This is in agreement with the fact that the type of situation shown in curve 1 of figure 3 is chiefly obtained in cases where the junction dislocation is sessile and should be unusual for the glissile intersections which are mainly encountered in hexagonal metals.

PHILOSOPHICAL TRANSACTIONS OF THE ROYAL SOCIETY A MATHEMATICAL, PHYSICAL & ENGINEERING SCIENCES

PHILOSOPHICAL TRANSACTIONS OF THE ROYAL SOCIETY A MATHEMATICAL, PHYSICAL & ENGINEERING SCIENCES

Downloaded from rsta.royalsocietypublishing.org

(e) *The effect of recovery on the flow stress*

If the forest intersection mechanism within cell walls controls the flow stress we should expect the flow stress to be dependent only on the dislocation density in the walls. However, Keh (1962) has observed that the flow stress of iron with a given dislocation density is lower if the iron has been recovered at 550 °C than if it is in the cold worked state. This supports the theory of Li (1961) that the long-range stress from cell walls contributes an appreciable part of the flow stress in iron, since the long-range stresses should be relaxed during recovery.

7. Discussion

From (3), (4) and (5) we see that purely random types of dislocation forest cannot account for the observed flow stress of cold worked metals, but that non-random types of dislocation tangle could act as effective obstacles or barriers to certain types of dislocations while allowing others to pass through. Such non-random tangles or cell walls are expected to develop during straining owing to the stability of attractive intersections being greater than that of repulsive ones.

The subsidiary evidence reviewed in (6) shows that there is considerable support for the importance of the forest mechanism in f.c.c. and h.c.p. metals, especially in the form developed above. For b.c.c. metals the evidence is less conclusive; there is good agreement between calculated and observed flow stresses but the orientation dependence of the work hardening is not well known. Although the absolute magnitudes of the calculated flow stresses may be somewhat in error, the ratio between the values for f.c.c. and b.c.c. metals should be reasonably accurate, since the same approximations have been used for both. It is therefore not possible to suppose that the forest mechanism accounts for most of the flow stress in the case of f.c.c. metals but not in the case of b.c.c. metals. Further examination is clearly required of the strain hardening characteristics of b.c.c. metals to establish whether the forest mechanism is applicable.

Despite the lack of some vital evidence there is little reason to doubt that the forest mechanism is important. This is especially so in polycrystalline metals showing a pronounced cellular structure at high strains. The mechanism accounts satisfactorily for the build-up of cell walls of the type observed. Also the low density of dislocations in the cell interiors suggests that moving dislocations are mostly stopped at the cell walls. There is no reason to suppose that the positions of cell walls coincide with regions of high internal stress field from other dislocation arrays, so that the dislocations must be stopped predominantly by interaction with other dislocations in the cell walls. These interactions will be predominately of the type discussed in the present paper, although in addition there will be some contribution from the interactions with non-intersecting dislocations, e.g. parallel ones on neighbouring glide planes.

8. Summary and conclusions

1. The behaviour of attractive dislocation intersections under stress has been analysed for a wide variety of possible cases in f.c.c. and b.c.c. crystals, the results of the f.c.c. case being also partly applicable to h.c.p. crystals. In particular the effect of the angular configuration of the intersection has been examined, the results being expressed in a series

Downloaded from rsta.royalsocietypublishing.org

of contour diagrams showing the values of the stresses required to break junctions of all possible angular parameters ϕ_1 and ϕ_2.

2. From these contour diagrams a series of average breaking stresses have been computed allowing for the probability of intersections of different angular configurations.

3. More physically realistic values of the limiting resistances of different types of forest to the passage of a glissile dislocation have been calculated using a new model, from which it has been shown that the averages hitherto used do not give an accurate estimate of the forest contribution to the flow stress.

4. In the case of a random forest of mean spacing l, the flow-stress contribution from attractive intersections has been shown to be 0·13 (Gb/l) for f.c.c. crystals and 0·09 (Gb/l) for b.c.c. crystals. At temperatures where thermal fluctuations supply the energy required to form intersection jogs, the weaker repulsive interactions contribute little to the forest flow stress.

5. At low temperatures an additional stress is required to form intersection jogs on the dislocations as they separate. This is added to the long-range intersection stress in the case of repulsive intersections, but the jog effect is shown to be appreciably smaller in the case of attractive intersections.

6. In view of the greater strength of attractive intersections than repulsive ones, it is proposed that dense dislocation networks will build up on straining in which most of the dislocations present are of two types that make attractive intersections with each other. Such a network would have a greater resistance to the passage of similar dislocations than a random forest of the same spacing, and it would allow dislocations of other Burgers vectors to pass through easily.

7. The resistance posed by such non-random cell walls (0·26 (Gb/l) and 0·18 (Gb/l) for f.c.c. and b.c.c. metals respectively) is in good agreement with the observed increases in flow stress due to strain hardening if l is taken as the experimentally observed spacing of dislocations in the cell walls.

8. In f.c.c. and h.c.p. metals a forest hardening mechanism of the above type is consistent with experimental observations on the orientation dependence of the initial work hardening rate in single crystals, the temperature dependence of the flow stress, the Bauschinger effect and the unloading yield point.

9. In b.c.c. metals the available evidence on the orientation dependence of strain hardening, on the temperature sensitivity of the flow stress and on the effect of recovery on the flow stress is inconclusive, but in general it is consistent with the proposed forest mechanism. In particular it is considered probable that the forest mechanism accounts for the build-up of the cellular type of structure in these metals and that attractive intersections in the cell walls must account largely for the trapping of dislocations in these regions.

The work described above has been carried out as part of the research programme of the National Physical Laboratory and this paper is published by permission of the Director of the Laboratory.

The authors desire to acknowledge the assistance rendered by Mr G. T. Anthony of the Mathematics Division who programmed some of the calculations for the computer.

PHILOSOPHICAL TRANSACTIONS OF THE ROYAL SOCIETY A MATHEMATICAL, PHYSICAL & ENGINEERING SCIENCES

PHILOSOPHICAL TRANSACTIONS OF THE ROYAL SOCIETY A MATHEMATICAL, PHYSICAL & ENGINEERING SCIENCES

Downloaded from rsta.royalsocietypublishing.org

Appendix A. Symmetrically stressed junctions

When $\beta_1 = \beta_2 = \beta$ and $\beta_3 = 0$ and $\zeta_1 = \zeta_1' = \zeta_2 = \zeta_2' = 1$ equations (7) reduce to

$$f_1(\epsilon_P, \gamma, \phi_1, \phi_2) \equiv (-\sin\phi_1 + \sin\phi_2)\,\beta\gamma + (\epsilon_P + \cos\phi_1)\,[(1 + 2\epsilon_P\cos\phi_1 + \epsilon_P^2)^{-1} - \beta^2\gamma^2]^{\frac{1}{2}} + (\epsilon_P + \cos\phi_2)\,[(1 + 2\epsilon_P\cos\phi_2 + \epsilon_P^2)^{-1} - \beta^2\gamma^2]^{\frac{1}{2}} - A = 0, \quad \text{(A 1)}$$

together with the symmetry relations:

$$f_1(\epsilon_P, \gamma, \phi_1, \phi_2) = f_1(\epsilon_P, -\gamma, -\phi_1, \phi_2) = f_1(\epsilon_P, -\gamma, \phi_2, \phi_1) = -f_2(-\epsilon_Q, -\gamma, \phi_1, \phi_2).$$

From these the symmetry relations (9) can be simply deduced. It is possible to obtain simple analytical solutions of (A 1) when $\phi_1 = \phi_2 = \phi$ and $\phi_1 = -\phi_2 = \phi$. In the first case it can readily be shown that:

$$\epsilon_P = -\cos\phi + [(8\beta^2\gamma^2)^{-1} \times \{4 - A^2 - 4\beta^2\gamma^2\sin^2\phi \pm [A^2 - 4(1 + 4\beta\gamma\sin\phi)^2]^{\frac{1}{2}}\,[A^2 - 4(1 - 4\beta\gamma\sin\phi)^2]^{\frac{1}{2}}\}]^{\frac{1}{2}}. \quad \text{(A 2)}$$

If $A > 2$ there are no real solutions, as would be expected from inequality (2). The co-ordinates of P_0 and Q_0, corresponding to $\gamma = 0$ are given by

$$\left.\begin{matrix}\epsilon(P_0)\\ \epsilon(Q_0)\end{matrix}\right\} = \mp\cos\phi \pm \frac{A\sin\phi}{\sqrt{(4 - A^2)}},$$

and the co-ordinates of the turning points on the $\gamma(\epsilon_P)$ curve are

$$\epsilon_P = -\cos\phi + A^{\frac{1}{2}}(2 - A)^{-\frac{1}{2}}\sin\phi$$

and

$$\beta\gamma = \pm\tfrac{1}{2}(2 - A)\operatorname{cosec}\phi.$$

From equation (A 2) it is evident that the curve for the P node lies entirely to the right of P_0, that it is symmetrical with respect to the ϵ_P axis, i.e. $\epsilon_{P(\gamma)} = \epsilon_{P(-\gamma)}$, and that $\gamma \to 0$ as $\epsilon_P \to +\infty$. It is shown schematically in figure 8 as curve a. The dashed curve corresponds to dislocation arcs which are greater than semicircles. The point P_0' on this second curve is of no physical significance since it would correspond to an arc of zero curvature and infinite length. Further, since the two arcs do not intersect and since the equilibrium configuration under zero stress is described by the point P_0 the subsequent change in the configuration with stress must be described only by the full curve.

In the second case it can be shown that the curve $\gamma = \gamma(\epsilon_P)$ has two branches

$$\epsilon_P = -\cos\phi + \alpha(\gamma) \quad \text{if} \quad \beta\gamma > -\tfrac{1}{2}A\operatorname{cosec}\phi,$$
$$\epsilon_P = -\cos\phi - \alpha(\gamma) \quad \text{if} \quad \beta\gamma < -\tfrac{1}{2}A\operatorname{cosec}\phi,$$

where

$$\alpha(\gamma) = [(8\beta^2\gamma^2)^{-1}\{4 - A^2 - 4A\beta\gamma\sin\phi - 8\beta^2\gamma^2\sin^2\phi \pm (4 - A^2)^{\frac{1}{2}}(4 - [A + 4\beta\gamma\sin\phi]^2)^{\frac{1}{2}}\}]^{\frac{1}{2}}.$$

These branches are shown as the full lines (b) in figure 8 which end at the points E_1 and E_2. The turning points are

$$P_m'\colon \epsilon_P = -\cos\phi - \left(\frac{2 - A}{2 + A}\right)^{\frac{1}{2}}\sin\phi, \quad \beta\gamma = -\tfrac{1}{4}(2 + A)\operatorname{cosec}\phi;$$

$$P_m\colon \epsilon_P = -\cos\phi + \left(\frac{2 + A}{2 - A}\right)^{\frac{1}{2}}\sin\phi, \quad \beta\gamma = \tfrac{1}{4}(2 - A)\operatorname{cosec}\phi.$$

Downloaded from rsta.royalsocietypublishing.org

The dashed curve corresponds to dislocation arcs which are greater than semicircles. The point E_1 is always to the left of the turning point P'_m and it is therefore, from the previous equilibrium discussion, associated with an unstable configuration. This termination of the $\gamma(\epsilon_P)$ curve is not therefore physically significant. Further, since the point E_2 is not on an arc of the $\gamma(\epsilon_P)$ curve passing through P_0 it too is of no significance. From the symmetry of the $\gamma(\epsilon_P)$ and $\gamma(\epsilon_Q)$ curves it follows that only the turning point corresponding to the lower value of $|\beta\gamma|$ is significant.

The values of γ_f for small values of ϕ_1 and ϕ_2 can be calculated from these special cases as follows. As shown above:

$$\beta\gamma_f \equiv \beta\gamma_m \simeq (2-A)/2\phi \quad \text{when} \quad \phi_1 = \phi_2 = \phi;$$

and

$$\beta\gamma_f \equiv \beta\gamma_m \simeq (2-A)/4\phi \quad \text{when} \quad \phi_1 = -\phi_2 = \phi.$$

When we combine these results with the symmetry relations (9) it follows that $\beta\gamma_f$ must to the first approximation be of the form:

$$\beta\gamma_f \simeq (2-A)\,(a\phi_1^2 + b\phi_1\phi_2 + a\phi_2^2)^{-\frac{1}{2}};$$

and from the special cases $a = 5$ and $b = 6$. The quadratic form is positive definite so that the contours $\beta\gamma_f =$ constant are ovals.

The behaviour of the reactions for other values of ϕ_1 and ϕ_2 were calculated on a computer using an iterative program based on the 'regula falsi' method of root extraction. The calculation of the numerators in $\langle\beta\gamma_f\rangle$ and $\langle\beta\gamma_f|\sin\phi_1|\rangle$ are slightly complicated by the presence of the singularity in $\beta\gamma_f$ at $\phi_1 = \phi_2 = 0$ and it is divided into two parts. For $|\phi_1;\phi_2| \geqslant \frac{1}{18}\pi$ the integrals were evaluated numerically using the two-dimensional form of Simpson's rule; for $0 < |\phi_1;\phi_2| \leqslant \frac{1}{18}\pi$ the integrals were evaluated using the analytical approximation for $\beta\gamma_f$. This second integral was calculated as follows: transform to polar co-ordinates r and θ, where the polar angle θ is zero along the line $\phi_1 = \phi_2$. The integral then becomes of the form

$$I \equiv 2\sqrt{2}(2-A)\int\int \frac{\mathrm{d}r\,\mathrm{d}\theta}{\sqrt{1+3\sin^2\theta}}$$

integrated over the triangle bounded by the points with polar co-ordinates $(0;0)$; $(\sqrt{2}\,X;0)$ and $(\sqrt{2}\,X;\frac{1}{2}\pi)$: where $0 \leqslant |\phi_1;\phi_2| \leqslant X$: in this case '$X$' would be $\frac{1}{18}\pi$. The integral can be conveniently evaluated by dividing the integration range into three parts defined by the inequalities

$$\left.\begin{matrix} 0 \leqslant r \leqslant X \\ 0 \leqslant \theta \leqslant \frac{1}{2}\pi \end{matrix}\right\} \quad \left.\begin{matrix} X \leqslant r \leqslant \sqrt{2}\,X \\ 0 \leqslant \theta \leqslant \theta_1 \end{matrix}\right\} \quad \begin{matrix} X \leqslant r \leqslant \sqrt{2}\,X, \\ \frac{1}{2}\pi - \theta_1 \leqslant \theta \leqslant \frac{1}{2}\pi, \end{matrix}$$

where $r(\cos\theta_1 + \sin\theta_1) = \sqrt{2}\,X$. The integrals corresponding to these three areas can then be evaluated in terms of Jacobian Elliptic functions. The integral I can then be written as:

$$I = \sqrt{2}(2-A)\left\{X\,\mathrm{sn}^{-1}(1\,|\,\tfrac{3}{4}) + \int_X^{\sqrt{2}X} [K - \mathrm{cn}^{-1}(\sin\theta_1\,|\,\tfrac{3}{4}) + \mathrm{cn}^{-1}(\cos\theta_1\,|\,\tfrac{3}{4})]\,\mathrm{d}r\right\}.$$

In this expression the integrand was evaluated using elliptic function tables (Milne-Thomson 1950), for different values of θ_1. The integral with respect to 'r' was then calculated numerically.

Downloaded from rsta.royalsocietypublishing.org

The corresponding integral I' for the weighted average was calculated as follows:

$$I' \simeq 2(2-A)\iint \frac{r(\cos\theta+\sin\theta)}{\sqrt{1+3\sin^2\theta}}\,\mathrm{d}r\,\mathrm{d}\theta$$

integrated over the rectangle bounded by the points with polar co-ordinates $(X;-\frac{1}{4}\pi)$, $(\sqrt{2}X;0)$ $(\sqrt{2}X;\frac{1}{2}\pi)$ and $(X;\frac{3}{4}\pi)$. It can then be easily shown that it reduces to

$$I' \simeq \frac{2}{\sqrt{3}}(2-A)\left[\tfrac{1}{2}X^2\{\sin^{-1}\sqrt{\tfrac{3}{8}}+\sinh^{-1}\sqrt{\tfrac{3}{2}}\}\right]+\int_X^{\sqrt{2}X} r\left\{\sin^{-1}\left(\frac{\sqrt{3}}{2}\sin\theta_1\right)+\sinh^{-1}(\sqrt{3}\sin\theta_1)\right\}\mathrm{d}r.$$

Appendix B. Asymmetrically stressed junctions

When $\beta_2 = \beta_3 = 0$, $\zeta_1 = \zeta_1'$ and $\zeta_2 = \zeta_2'$ equations (7) reduce to

$$f_1(\epsilon_P,\gamma,\phi_1,\phi_2) \equiv -\zeta_1\sin\phi_1\beta_1\gamma+(\epsilon_P+\zeta_1\cos\phi_1)\left[(\epsilon_P^2+2\epsilon_P\zeta_1\cos\phi_1+\zeta_1^2)^{-1}-\beta_1^2\gamma^2\right]^{\frac{1}{2}} + (\epsilon_P+\zeta_2\cos\phi_2)\left[\epsilon_P^2+2\epsilon_P\zeta_2\cos\phi_2+\zeta_2^2\right]^{-\frac{1}{2}}-A=0, \quad \text{(B 1)}$$

together with the symmetry relations

$$f_1(\epsilon_P,\gamma,\phi_1,\phi_2) = f_1(\epsilon_P,-\gamma,-\phi_1,\phi_2) = f_1(\epsilon_P,\gamma,\phi_1,-\phi_2) = -f_2(-\epsilon_Q,-\gamma,\phi_1,\phi_2).$$

From these the symmetry relations (10) can be deduced.

Rationalizing equation (B 1) and solving the resulting quadratic for $\beta_1\gamma$ gives

$$\beta_1\gamma = \frac{-\zeta_1\sin\phi_1\,.\,Q\pm(\epsilon_P+\zeta_1\cos\phi_1)\,(1-Q^2)^{\frac{1}{2}}}{\zeta_1^2+2\zeta_1\epsilon_P\cos\phi_1+\epsilon_P^2}, \quad \text{(B 2)}$$

where $$Q \equiv A-(\epsilon_P+\zeta_2\cos\phi_2)\,(\epsilon_P^2+2\epsilon_P\zeta_2\cos\phi_2+\zeta_2^2)^{-\frac{1}{2}}.$$

The values of $\beta_1\gamma$ can thus be calculated directly and the values of $\beta_1\gamma_f$ deduced numerically. The behaviour of $\beta_1\gamma_f$ is however peculiar for certain values of ϕ_1 and ϕ_2 and this is discussed analytically.

(*a*) If $\phi_1 = 0$ then $-\zeta_1 \leqslant \epsilon_P \leqslant +\zeta_1$ and

$$\epsilon_P = -\zeta_2\left\{-\cos\phi_2+\frac{A-1}{\sqrt{A(2-A)}}\sin\phi_2\right\} \quad \text{when} \quad \gamma=0.$$

Along this axis the behaviour depends on the ratio $\eta \equiv \zeta_1/\zeta_2$.

(i) $\eta > 1$. Then $\epsilon_P \to -\zeta_2$ as $\phi_2 \to 0$ and for small values of ϕ_2; $\epsilon_P \simeq \zeta_2 + a|\phi_2|^P$. Differentiating equation (B 2), substituting this value of ϵ_P and equating the result to zero it can be shown that

$$\zeta_1\beta_1\gamma_m \simeq \pm\frac{[A(2-A)]^{\frac{1}{2}}}{\eta-1}\left\{1-\left[\frac{(A-1)\,\phi_2^2}{A(2-A)\,(\eta-1)^2}\right]^{\frac{1}{3}}\right\} \quad \text{if} \quad A \neq 1$$

and

$$\simeq \pm\frac{1}{\eta-1}\left\{1-\frac{1}{4}\left(\frac{2\phi_2}{\eta-1}\right)^{\frac{4}{3}}\right\} \quad \text{if} \quad A=1,$$

(ii) $\eta < 1$. In this case the positions of P_0 and Q_0 lie outside the segment A_1A_1' if $\phi_2 < \phi_c$, where

$$\cos\phi_c = \eta A(2-A)+(A-1)\left[1-A(2-A)\,\eta^2\right]^{\frac{1}{2}}. \quad \text{(B 3)}$$

When $\phi_2 = \phi_c$ and $\gamma = 0$, $\epsilon_P = -\zeta_1$. If $\phi_2 = \phi_c + \Delta\phi_2$ the maximum value of γ occurs at $\epsilon_P = -\zeta_1 + \Delta\epsilon_P$, where

$$\Delta\epsilon_P \simeq \frac{\pm\zeta_2\sin^{\frac{2}{3}}\phi_c}{[2(\zeta_2-\zeta_1\cos\phi_c)\,\Delta\phi_2]^{\frac{1}{3}}}\,(\zeta_1^2-2\zeta_1\zeta_2\cos\phi_c+\zeta_2^2)^{\frac{1}{3}}.$$

Downloaded from rsta.royalsocietypublishing.org

Thus for these junctions $\gamma_m \propto (\phi_2 - \phi_c)^{-\frac{1}{2}}$ if $|\phi_2| > \phi_c$ and γ_m is infinite, or undefined, if $|\phi_2| < \phi_c$. When $A = 1$, $\cos\phi_c = \eta$ and in this case there is no anomaly.

(*b*) If $\phi_2 = 0$ it can be shown that the values of ϵ_P and γ given by equation (*B* 2) which satisfy equation (B 1) are

$$\begin{aligned} \epsilon_P &= -\zeta_1 \cos\phi_1 + \alpha(\gamma) \quad \text{if} \quad \zeta_1\beta_1\gamma \geqslant (1-A)\operatorname{cosec}\phi_1, \\ &= -\zeta_1 \cos\phi_1 - \alpha(\gamma) \quad \text{if} \quad \zeta_1\beta_1\gamma \leqslant (1-A)\operatorname{cosec}\phi_1, \end{aligned}$$

where $$\alpha(\gamma) = \frac{1}{2\beta_1\gamma}[\{A(2-A)\}^{\frac{1}{2}} \pm \{(A + 2\beta_1\gamma_1\zeta\sin\phi_1)\,(2 - A - 2\beta_1\zeta_1\gamma\sin\phi_1)\}^{\frac{1}{2}}].$$

This curve is similar to that shown in figure 8 and the discussion of its properties given in appendix A is also relevant here. The turning points occur at

$$\epsilon_P = -\zeta_1\left\{\cos\phi_1 - \left(\frac{2-A}{A}\right)^{\frac{1}{2}}\sin\phi_1\right\} \quad \text{with} \quad \zeta_1\beta_1\gamma_m = -\tfrac{1}{2}A\operatorname{cosec}\phi_1$$

and $$\epsilon_P = -\zeta_1\left\{\cos\phi_1 + \left(\frac{A}{2-A}\right)^{\frac{1}{2}}\sin\phi_1\right\} \quad \text{with} \quad \zeta_1\beta_1\gamma_m = \tfrac{1}{2}(2-A)\operatorname{cosec}\phi_1. \tag{B 4}$$

For $1 \leqslant A \leqslant 2$ the significant value, i.e. the lowest magnitude of γ_m, is the second one; provided that $\eta < 1$. If, however, $\eta > 1$ the positions of P_0 and Q_0 lie outside the segment A_2A_2' if $\phi_1 < \phi_c'$, where

$$\cos\phi_c' = \frac{1}{\eta}A(2-A) + (A-1)\left[1 - \frac{A(2-A)}{\eta^2}\right]^{\frac{1}{2}}. \tag{B 5}$$

No reactions occur if $\phi_1 < \phi_c'$ and $\phi_2 = 0$ but if ϕ_2 is infinitesimally close to zero they do occur and their breaking stresses are given by (B 4). This discontinuous behaviour is a consequence of assuming that A_2 and A_2' are points.

The contours of constant γ_f are shown in figure 6 for $\eta > 1$. The average and weighted averages for $\eta > 1$ can be calculated numerically without trouble from the set of indeterminate reactions along the ϕ_1 axis. For $\eta < 1$, however, the line singularity along the ϕ_2 axis implies that $\langle\gamma_f\rangle$ and $\langle\gamma_f|\sin\phi_2|\rangle$ are infinite, though $\langle\gamma_f|\sin\phi_1|\rangle$ is defined and can be calculated numerically.

When $\eta = 1$ the treatment given above is no longer valid and it must be modified. In this case there are no line discontinuities and a proper treatment of the averages is both simpler and more satisfactory. If $\phi_1 = 0$ the value of ϵ_P for which γ is a maximum was obtained by a similar method to that used when $\eta > 1$.

It is found that

$$\epsilon_P \simeq -1 + 0{\cdot}582\phi_2 \quad \text{and} \quad \gamma_m \simeq 0{\cdot}957/\phi_2 \quad \text{when} \quad A \neq 1,$$

but $$\epsilon_P \simeq -1 + \phi_2^2 \quad \text{and} \quad \gamma_m \simeq \phi_2^{-\frac{3}{2}} \quad \text{when} \quad A = 1.$$

If $\phi_2 = 0$ $\gamma_m = \frac{1}{2}(2-A)\operatorname{cosec}\phi_1$, as before so that if $A \neq 1$ the symmetry relations (10) show that for small values of ϕ_1 and σ_2 γ_m must be of the form

$$\gamma_m = (a\phi_1^2 + b\phi_2^2)^{-\frac{1}{2}}.$$

If $A = \frac{4}{3}$ $a \simeq 9$ and $b = 1$. The contribution of the singularity to the average of γ_f can be calculated in terms of elliptic functions as indicated in appendix A. The calculation for the weighted averages is also similar to that in appendix A.

Downloaded from rsta.royalsocietypublishing.org

If however $A = 1$ the symmetry and results for $\phi_1 = 0$ and $\phi_2 = 0$ imply that for small values of ϕ_1 and ϕ_2 γ_m must be of the form

$$\gamma_m = (a\phi_1^4 + b\phi_1^2\phi_2^2 + c\phi_2^6)^{-\frac{1}{4}}. \tag{B 6}$$

To determine b it is necessary to calculate γ_m when $\phi_1 = \phi_2 = \phi$. This was done by substituting the power series $\epsilon_P = -1 + r_1\phi + r_2\phi^2 + \ldots$ and $\gamma_m^{-1} = S_1\phi + S_2\phi^2 + \ldots$ into the equation (B 2) and its derivative put equal to zero. Equating powers of ϕ to zero gave a set of simultaneous non-linear equations which could be solved in sequence to give the 'a' and 'b' coefficients. The first two pairs were: $r_1 \simeq 1{\cdot}47$, $r_2 = \frac{1}{2}$, $S_1 \simeq 2{\cdot}41$ and $S_2 = 0$. The coefficients a, b and c in equation (B 6) are then approximately: $a = 16$, $b = 28$, $c = 1$.

The contribution to the average from the singularity was obtained by transforming to polar co-ordinates.

Thus

$$\int_{-x}^{x}\int_{-x}^{x} \gamma_f \,\mathrm{d}\phi_1\,\mathrm{d}\phi_2 = 4\left\{\int_0^{x\sec\theta}\int_0^{\pi/4} + \int_0^{x\,\mathrm{cosec}\,\theta}\int_{\pi/4}^{\pi/2}\right\}(16 - 4\sin^2\theta - 12\sin^4\theta + r^2\sin^6\theta)^{-\frac{1}{4}}\,\mathrm{d}r\,\mathrm{d}\theta.$$

The integral was evaluated numerically with respect to 'r' and then with respect to θ. The value was found to be $1{\cdot}074$. Similar integrals were obtained and evaluated for the weighted averages.

If $\zeta_1 \to \infty$ equation (B 2) shows that $\beta_1\gamma \to 0$ for all values of ϕ_1 and ϕ_2. However, if $\zeta_2 \to \infty$ the critical value ϕ_c is given by $\cos\phi_c = A - 1$ and occurs on the boundary $\gamma_f = 0$. The $\gamma(\epsilon)$ curve has two branches, as in figure 8, the physically relevant one being

$$\beta_1\gamma = \frac{-\zeta_1\sin\phi_1(A - \cos\phi_2) + (\epsilon_P + \zeta_1\cos\phi_1)\,[1 - (A - \cos\phi_1)^2]^{\frac{1}{2}}}{\epsilon_P^2 + 2\epsilon_P\zeta_1\cos\phi + \zeta_1^2},$$

with

$$\epsilon_P \geqslant -\zeta_1\cos\phi_1 - \frac{\zeta_1\sin\phi_1}{A - \cos\phi_2}\,[1 - (A - \cos\phi_2)^2]^{\frac{1}{2}}.$$

The breaking stress is given by

$$\beta_1\gamma_m = \frac{1 - A + \cos\phi_2}{2\zeta_1\sin\phi_1},$$

and the only meaningful average is the weighted one with respect to $\sin\phi_1$. This is given by

$$\langle\beta_1\gamma_f|\sin\phi_1|\rangle = \frac{2}{\zeta_1}\int_0^{\cos^{-1}(A-1)} (1 - A + \cos\phi_2)\cos^{-1}(A - \cos\phi_2)\,\mathrm{d}\phi_2$$

and can easily be evaluated numerically.

Appendix C. Glissile junctions

It is possible to obtain simple analytical solutions of equations (7) for glissile junctions having the following parameters:

$$\beta_1 = \beta_2 = \beta;\quad \beta_3;\quad \zeta_1 = \zeta_1' = \zeta_2 = \zeta_2' \quad\text{and}\quad \phi_1 = -\phi_2 = \phi.$$

In this case equations (7) reduce to

$$f_1(\epsilon_P;\,\epsilon_Q;\,\gamma;\,\phi) \equiv 2(\epsilon_P + \cos\phi)\,[(1 + 2\epsilon_P\cos\phi + \epsilon_P^2)^{-1} - \beta^2\gamma^2]^{\frac{1}{2}} - A\{1 - [\beta_3\gamma(\epsilon_P - \epsilon_Q)]^2\}^{\frac{1}{2}} = 0$$

and

$$f_2(-\epsilon_P;\,-\epsilon_Q;\,\gamma;\,\phi) = -f_1(\epsilon_Q;\,\epsilon_P;\,\gamma;\,\phi).$$

Downloaded from rsta.royalsocietypublishing.org

It can then be shown that the solutions lie on arcs of the curves:

$$\epsilon_P = -\epsilon_Q,$$
$$\beta\gamma = \pm\frac{1}{2}\left[\frac{A^2-4(\epsilon_P+\cos\phi)^2\,(1+2\epsilon_P\cos\phi+\epsilon_P^2)^{-1}}{m^2A^2\epsilon_P^2-(\epsilon_P+\cos\phi)^2}\right]^{\frac{1}{2}},$$

where $m \equiv \beta_3/\beta$ defined by the inequalities

$$\epsilon_P > -\cos\phi,$$
$$h_1(\epsilon_P;\gamma) \equiv (1+2\epsilon_P\cos\phi+\epsilon_P^2)^{-1}-\beta^2\gamma^2 > 0,$$
$$h_2(\epsilon_P;\gamma) \equiv 1-4\beta_3^2\epsilon_P^2\gamma^2 > 0.$$

A number of forms for these curves are possible depending on the values of m and ϕ: these are shown in figure 9. The full curves refer to the P node and the dotted ones to the Q node.

Figure 9 (a) corresponds to the case

$$|m|A > 1 \qquad \frac{|m|}{A|m|+1} < \frac{\tan\phi}{\sqrt{(4-A^2)}}. \tag{C 1}$$

The arc P_1P_2 is bounded by the intersections of h_1 and h_2 with f_1. Here and in all the diagrams $\epsilon_P = -\cos\phi$ at P_1. The configurations represented by points on this arc cannot be reached by increasing the stress parameter from zero. When $\gamma = 0$ the nodes are at P_0 and Q_0 and when γ is increased they eventually meet at K.

Figure 9 (b) corresponds to the case

$$|m|A > 1 \qquad \frac{|m|}{A|m|+1} > \frac{\tan\phi}{\sqrt{(4-A^2)}}. \tag{C 2}$$

As in case (a), the isolated arc P_3P_4 is not attainable starting from zero stress. As γ is increased the nodes separate and when the turning points are reached the junction relaxes and the arc PQ becomes semicircular.

Figure 9 (c) is similar to the previous one except that the arc P_3P_4 has no turning point. This corresponds to the cases:

$$\left.\begin{aligned} |m|A = 1 \qquad & \frac{A\tan\phi}{\sqrt{(4-A^2)}} < \tfrac{1}{2}, \\ |m|A < 1 \qquad & \frac{|m|}{1-|m|A} > \frac{|m|}{1+|m|A} > \frac{\tan\phi}{\sqrt{(4-A^2)}}. \end{aligned}\right\} \tag{C 3}$$

In figure 9 (d): as in cases (a) and (b) the isolated arc P_1P_2 is not attainable from zero stress. The significant curve is similar to that obtained for sessile junctions, and this behaviour corresponds to the cases:

$$\left.\begin{aligned} |m|A = 1 \qquad & \frac{A\tan\phi}{\sqrt{(4-A^2)}} > \tfrac{1}{2}, \\ |m|A < 1 \qquad & \frac{|m|}{1-|m|A} > \frac{\tan\phi}{\sqrt{(4-A^2)}} > \frac{|m|}{1+|m|A}. \end{aligned}\right\} \tag{C 4}$$

The equilibria of the dislocation configurations represented by the curves in figure 9 are determined by the signs of the quantities

$$\frac{\partial f_1}{\partial \epsilon_P}, \quad \frac{\partial f_2}{\partial \epsilon_Q} \quad \text{and} \quad \left|\frac{\partial(f_1,f_2)}{\partial(\epsilon_P,\epsilon_Q)}\right|.$$

Downloaded from rsta.royalsocietypublishing.org

For the curves which begin at P_0 and Q_0 it has been shown in § 1 that up to the turning points the free energy is a minimum but that beyond it is not. This discussion can be extended to the isolated arcs P_1P_2, P_3P_4, etc. It can easily be shown that for the symmetrical glissile junction discussed here:

$$\frac{\partial f_1}{\partial \epsilon_P} = \frac{\partial f_2}{\partial \epsilon_Q} = -\frac{2}{Ah_2^{\frac{1}{2}}}\{2(\epsilon_P+\cos\phi)\,[h_1-(\epsilon_P+\cos\phi)^2\,(1+2\epsilon_P\cos\phi+\epsilon_P^2)^{-2}]+A^2\beta_3^2\gamma^2\epsilon_P\}, \quad \text{(C 5)}$$

$$\frac{\partial f_1}{\partial \epsilon_Q} = \frac{\partial f_2}{\partial \epsilon_P} = -2A\beta_3^2\gamma^2\epsilon_P h_2^{-\frac{1}{2}}, \quad \text{(C 6)}$$

$$\frac{\partial f_1}{\partial \gamma} = -\frac{\partial f_2}{\partial \gamma} = \frac{2\gamma\beta}{h_2^{\frac{1}{2}}}\{m^2A^2\epsilon_P^2-(\epsilon_P+\cos\phi)^2\} \quad \text{(C 7)}$$

and

$$\frac{\mathrm{d}\gamma}{\mathrm{d}\epsilon_P} = \left|\frac{\partial(f_1,f_2)}{\partial(\epsilon_P,\epsilon_Q)}\right| \Big/ \left|\frac{\partial(f_1,f_2)}{\partial(\epsilon_Q,\gamma)}\right| = \left(\frac{\partial f_1}{\partial \epsilon_Q}-\frac{\partial f_1}{\partial \epsilon_P}\right)\Big/\frac{\partial f_1}{\partial \gamma}. \quad \text{(C 8)}$$

For the arcs P_1P_2 in figures 9 (*a*) and (*d*) the quantities $m^2A^2\epsilon_P^2-(\epsilon_P+\cos\phi)^2$ and $\partial\gamma/\partial\epsilon_P$ are positive. Hence from relations (C 7) and (C 8): $\partial f_1/\partial\epsilon_Q-\partial f_1/\partial\epsilon_P>0$. A necessary condition for the free energy to be a minimum is that

$$\left|\frac{\partial(f_1,f_2)}{\partial(\epsilon_P,\epsilon_Q)}\right| = \left(\frac{\partial f_1}{\partial \epsilon_P}+\frac{\partial f_1}{\partial \epsilon_Q}\right)\left(\frac{\partial f_1}{\partial \epsilon_P}-\frac{\partial f_1}{\partial \epsilon_Q}\right)>0.$$

If this condition is satisfied then $\partial f_1/\partial\epsilon_P+\partial f_1/\partial\epsilon_Q$ must be negative but this is only possible if $\partial f_1/\partial\epsilon_P<0$. The free energies of all the dislocation configurations represented by points on the arc P_1P_2 are not therefore minima.

A similar argument can be used to prove the same result for the arc P_3P_4 in figure 9 (*c*) and for that part of the arc P_3P_4 in figure 9 (*b*) which is to the left of the minimum. To the right of the minimum $\mathrm{d}\gamma/\mathrm{d}\epsilon_P>0$ and $\partial f_1/\partial\gamma>0$ so that from (C 8) $\partial f_1/\partial\epsilon_Q-\partial f_1/\partial\epsilon_P<0$. If the Jacobian is positive then $\partial f_1/\partial\epsilon_P+\partial f_1/\partial\epsilon_Q$ is also, which is only possible if $\partial f_1/\partial\epsilon_P>0$. The configurations corresponding to this part of the arc P_3P_4 are therefore stable. However, if the minimum of the $\gamma(\epsilon_P)$ curve occurs when $\epsilon_P>0$ these stable configurations are not attained since when $\epsilon_P=\epsilon_Q=0$ the junction collapses. A necessary condition for the minimum to occur when $\epsilon_P<0$ is that

$$\left.\frac{\mathrm{d}\gamma}{\mathrm{d}\epsilon_P}\right|_{\epsilon_P=0} = -\frac{\partial f_1}{\partial \epsilon_P}\Big/\left.\frac{\partial f_1}{\partial \gamma}\right|_{\epsilon_P=0}>0, \quad \text{i.e.} \quad \left.\frac{\partial f_1}{\partial \epsilon_P}\right|_{\epsilon_P=0} = \frac{1}{A}\sec\phi(A^2-4\cos^4\phi)>0.$$

Since $\partial f_1/\partial\gamma<0$ for the arc P_3P_4. Combining this inequality with the condition (C 2), that the $\gamma(\epsilon_P)$ curve has a minimum, gives as necessary conditions $\frac{1}{2}A>\cos\phi>\sqrt{(\frac{1}{2}A)}$ and $(A-2)\,(3A-2)>0$. But $0<A\leqslant 2$ so the latter condition is $A<\frac{2}{3}$. For the reactions considered in this paper $A>\frac{2}{3}$ so that there are no cases of stable equilibrium on those parts of isolated arcs which can be attained.

References

Adams, M. A. & Cottrell, A. H. 1955 *Phil. Mag.* **46**, 1187.
Bailey, J. E. & Hirsch, P. B. 1960 *Phil. Mag.* **5**, 485.
Bailey, J. E. 1963 *Phil. Mag.* **8**, 223.
Baird, J. D. & Gale, B. 1960 *Congr. Int. Un. Crystallogr., Cambridge.*
Basinski, Z. S. 1959 *Phil. Mag.* **4**, 393.
Basinski, Z. S. 1960 *Aust. J. Phys.* **13**, 284.

PHILOSOPHICAL TRANSACTIONS OF THE ROYAL SOCIETY A MATHEMATICAL, PHYSICAL & ENGINEERING SCIENCES
PHILOSOPHICAL TRANSACTIONS OF THE ROYAL SOCIETY A MATHEMATICAL, PHYSICAL & ENGINEERING SCIENCES

Downloaded from rsta.royalsocietypublishing.org

Basinski, Z. S. & Christian, J. W. 1960 *Aust. J. Phys.* **13**, 299.
Barrett, C. S. 1953 *Structure of metals.* New York: McGraw-Hill.
Birnbaum, H. K. 1961 *Acta Metall.* **9**, 320.
Bolling, G. F. 1959 *Phil. Mag.* **4**, 537.
Carrington, W., Hale, K. F. & McLean, D. 1960 *Proc. Roy. Soc.* A, **259**, 203.
Clarebrough, L. M. & Hargreaves, M. E. 1959 *Progr. Metal Phys.*, Vol. 8. Pergamon Press.
Clarebrough, L. M. & Hargreaves, M. E. 1960 *Aust. J. Phys.* **13**, 316.
Conrad, H. & Schoek, G. 1960 *Acta Metall.* **8**, 791.
Conrad, H., Hays, L., Schoeck, G. & Wiedersich, H. 1961 *Acta Metall.* **9**, 367.
Conrad, H. & Frederick, S. 1962 *Acta Metall.* **10**, 1013.
Cottrell, A. H. 1953 *Dislocations and plastic flow in crystals.* Oxford University Press.
Cottrell, A. H. & Stokes, R. J. 1955 *Proc. Roy. Soc.* A, **233**, 17.
Dohi, H. 1959 *J. Sci. Hiroshima Univ.* A, **23**, 395.
Diehl, J. & Berner, R. 1960 *Z. Metallk.* **52**, 323.
Elam, C. F. 1935 *The distortion of metal crystals.* Oxford University Press.
Friedel, J. 1956 *Les Dislocations* Paris: Gauthier-Villars.
Friedel, J. 1959 *Internal stresses and fatigue in metals; General Motors Symposium.*
Friedel, J. 1963 *Electron microscopy and strength of crystals*, p. 605. New York: Interscience.
Friedel, J. 1964 *N.P.L. Conf. on 'The relation between structure and strength in metals and alloys'.* London: H.M.S.O.
Haasen, P. & Kelly, A. 1957 *Acta Metall.* **5**, 192.
Hirsch, P. B. 1959*a* *J. Inst. Metals.* **87**, 406.
Hirsch, P. B 1959*b* *Internal stresses and fatigue in metals; General Motors Symposium.*
Hirsch, P. B. 1964 *N.P.L. Conf. on 'The relation between structure and strength in metals and alloys'.* London: H.M.S.O.
Jaoul, B. & Gonzalez, D. 1960 *J. Mech. Phys. Solids*, **9**, 16.
Keh, A. S. 1962 *Direct observations of imperfections in crystals.* New York: Interscience.
Keh, A. S. & Weissmann, S. 1963 *Electron microscopy and strength of crystals*, p. 231. New York: Interscience.
Levinstein, H. J. & Robinson, W. H. 1964 *N.P.L. Conf. on 'The relation between structure and strength in metals and alloys'.* London: H.M.S.O.
Li, J. C. M. 1961 Discussion to A. S. Keh.
McQuillan, A. D. & McQuillan, M. K. 1956 *Titanium.* Butterworths.
Mader, S., Seeger, A. & Thieringer, H. M. 1964 *N.P.L. Conf. on 'The relation between structure and strength in metals and alloys'.* London: H.M.S.O.
Makin, M. J. 1958 *Phil. Mag.* **3**, 287.
Mitra, S. K., Osborne, P. W. & Dorn, J. E. 1961 *Trans. Met. Soc. A.I.M.E.* **221**, 1206.
Milne-Thomson, L. M. 1950 *Jacobian elliptic function tables.* New York: Dover.
Mordike, B. L. & Haasen, P. 1962 *Phil. Mag.* **7**, 459.
Mott, N. F. 1952 *Phil. Mag.* **43**, 1151.
Orowan, E. 1959 *Internal stresses and fatigue in metals. General Motors Symposium.*
Rapperport, E. J. 1955 *Acta Metall.* **3**, 208.
Saada, G. 1960*a* *Acta Metall.* **8**, 841.
Saada, G. 1960*b* Thèse Faculte des Sciences, Paris.
Seeger, A. 1958*a* *Dislocations and mechanical properties of crystals.* Lake Placid.
Seeger, A. 1958*b* *Handb. Phys.* p. 1. Berlin: Springer.
Schmid, E. & Boas, W. 1935 *Kristallplastizität.* Berlin: Springer.
Thornton, P. R. 1959 Thesis, Cambridge.
Venables, J. A. 1962 *Phil. Mag.* **7**, 1969.

PHILOSOPHICAL TRANSACTIONS OF THE ROYAL SOCIETY A MATHEMATICAL, PHYSICAL & ENGINEERING SCIENCES

PHILOSOPHICAL TRANSACTIONS OF THE ROYAL SOCIETY A MATHEMATICAL, PHYSICAL & ENGINEERING SCIENCES